DESIGN AND SIMULATIONS OF MICROWAVE FILTERS USING NON-UNIFORM TRANSMISSION LINE AND SUPERFORMULA

by

Zhaoyang Li

A Thesis

Submitted to the Faculty of Purdue University

In Partial Fulfillment of the Requirements for the degree of

Master of Science in Electrical and Computer Engineering

Department of Electrical and Computer Engineering

Hammond, Indiana

December 2019

THE PURDUE UNIVERSITY GRADUATE SCHOOL
STATEMENT OF COMMITTEE APPROVAL

Dr. Khair Al Shamaileh, Chair

Department of Electrical and Computer Engineering

Dr. Xiaoli Yang

Department of Electrical and Computer Engineering

Dr. Lizhe Tan

Department of Electrical and Computer Engineering

Approved by:

Dr. Vijay Devabhaktuni

This thesis is dedicated to the memory of my respectable grandfather

ACKNOWLEDGMENTS

I would like to express my appreciation and deep gratitude to my thesis professor Dr. Khair Al Shamaileh for his valuable and constructive suggestions during the planning and developing of this research work.

I would also like to extend my thanks to my parents for supporting me consistently during the years of studying abroad.

Last but not least, I would like to thank the other committee members, for their helpful comments and meaningful suggestions.

TABLE OF CONTENTS

LIST OF TABLES

LIST OF FIGURES

ABSTRACT

In this study, a novel and systematic methodology for the design and optimization of lowpass filters (LPFs), and multiorder-bandpass filters (BPFs) are proposed. The width of the LPF signal traces consistently follow Fourier truncated series, and the thickness of the substrate as well. By studying different lengths and other physical constraints, the design meets predefined electrical requirements. Moreover, superformula is used in split ring resonators (SRRs) designs to obtain a BPF response and significant structural compactness.

Non-uniform transmission lines, as well as superformula equations, are programmed in MATLAB, which is also used for analytical validations. Traces are drawn in AutoCAD. The substrate of LPF is constructed in Pro/e. Finally, the optimized layouts are imported to Ansys High Frequency Structure Simulation (HFSS) software for simulation and verification. Non-uniform LPFs are optimized over a range of 0-6 GHz with cutoff frequency 3.5 GHz. Superformula implemented multiorder-BPFs are optimized with cutoff frequency of 1.1 GHz.

Keywords—low pass filter (LPF), microstrip line, multiorder-bandpass filter, printed circuit board (PCB) trace, split ring resonator (SRR), superformula.

CHAPTER 1. INTRODUCTION

1.1 Introduction

In microwave engineering, the operation frequency ranges from 300 MHz to 300 GHz, and the physical size of the circuit is close to the signal wavelength. Here, circuit design and construction are much more complicated because standard circuit theory cannot be used. Thus, conventional lumped circuit components, such as inductors, capacitors, and resistors (i.e., LRC), cannot predict signal integrity and cannot respond as expected at such high frequencies. In order to move signals from one port to another, conventional wires are replaced by other types of "guided media." As a result, distributed transmission lines such as microstrip lines are utilized in high frequency applications, and microwave theory.

1.2 Thesis Scope

Microwave engineering is to study and design microwave circuits and components by applying theories like transmission lines. Meanwhile, analyzing the performance of the components, such as LPFs and BPFs in this thesis is also required. The width, of the LPF transmission line, as well as the thickness of the substrate are following a Fourier truncated series expansion, and square shaped conventional SRR is replaced by the superformula shape for BPF application. Obtaining the optimum passband and stopband response for LPFs and BPFs is the main purpose of the optimization-driven procedure. The physical and electrical constraints (i.e. minimum-maximum signal trace widths, electrical performances) are under consideration. After the optimized models (both LPFs and BPFs) are achieved using MATLAB, Pro/e, and AutoCad, a full-wave simulation (HFSS) is performed. All of the simulation results are used to justify of the optimized structures.

1.3 Methodology

This thesis employs the technique of non-uniform transmission lines (NTLs) applied in LPF, as well as superformula SRR-BPF. In LPFs, in order to get minimum physical area, width and length of the NTL, and thickness of the substrate are optimized in MATLAB. AutoCad is used to draw the transmission lines and Pro/e is used to construct 3D substrate models. In BPF designs,

superformula curves are generated in MATLAB and drawn in AuotCad. HFSS is used to parametric simulation. Compared with conventional designs: ***by keeping a better (or same) electrical response, this thesis reduces physical length of LPF, and physical area of conventional SRR-BPF.***

1.4 Literature Survey

Microstrip is a type of electrical transmission line which can be fabricated using printed circuit board technology which widely used in communication area to convey microwave-frequency signals, which were descripted in [1-5]. In [1], microstrip transmission lines with finite-width dielectric and ground plane were presented. In [2], it discussed fundamental transmission properties of the microstrip line in view of varying the length, which will be used for d for device formation/fabrication and highest frequency of operation. In [3], a compact ultra-wideband (UWB) monopole microstrip antenna, with dual band-notched characteristics for short distance wireless applications were explored. In [4], several types of print circuit board (PCB) techniques were introduced and analyzed. PCB replaced with Printed Circuit Structure (PCS) was discussed in [5], which will move beyond 2D stacking, to make 3D packages and to utilize the 3-dimension directly. However, the objective of size reduction is not obviously mentioned in [1-5].

The LPF design was always seen as an attractive topic in the communication engineering area [6-18]. In [6], LPF with compact size was proposed to get sharp skirt characteristic and wideband suppression. In [7], a five-pole Butterworth transverse resonance type LPF (TR-LPF) was used to get sharp-cut-off frequency. A design of compact, sharp rejection microstrip LPF with wide-stopband was presented in [8]. In [9], the design of microwave LPF by using microstrip layout was proposed. However, the cutoff frequency that it measured was not matched with the simulation. In [10], a compact microstrip LPF with a very wide passband was designed based on generalized Chebyshev filter prototype of nine degree, this gains one transmission zero at edge of the passband which enhanced selectivity. In [11], a new compact microstrip LPF with sharp roll-off and ultrawide stopband using funnel and triangular patch resonators was proposed. In [12], defected ground structure (DGS) was proposed for LPF applications, whose structure exhibits wideband attenuation without increasing the circuit size, as compared to the conventional filter. In [13], a LPF with wide stopband using four non-uniform cascaded DGS

units consists of a combination of three isosceles U-shaped DGSs, where analyzed in terms of an equivalent RLC circuit model. In [14], a microstrip LPF based on transmission line elements for UWB medical applications was proposed. The filter was designed to exhibit an elliptic function response with equal ripple in the passband and the rejection band. In [15], a design technique for a stepped impedance microstrip LPF was presented by using the artificial neural network (ANN) modeling method. In [16], a LPF of a pair of feed lines with spurline resonators and a compact step impedance hairpin resonator. In [17], a detailed design of passive one pole, two pole, four pole lowpass Butterworth filter was presented. However, the frequency response was not perfectly matching with the analytical result. In [18], the design of a compact Butterworth LPF was proposed.

Comparing with uniform-transmission lines, non-uniform transmission lines (NTLs) is an open research area [19-23]. In [19], ultra-compact switchable BPF-LPF with wide stopband and good attenuation characteristics was proposed. In [20], nonhomogeneous transmission lines, which have position varying quantities, can be used to design LPFs. In [21], NTLs were analyzed with a numerical method based on the implementation of method of moment (MOM). Although the results were good comparing with uniform transmission lines (UTLs), the physical characteristics were not improved. In [22], a new design of stepped-impedance LPF in microstrip technology based on the use of non-uniform sections was presented. In [23], a 'roller coaster' transmission lines with thickness and width-modulated displays an expected electromagnetic result.

Microstrip BPFs have been researched in the past decades [24-31]. In [24], a slow-wave open-loop resonator was applied in BPF design. The slow-wave open-loop resonators make the filter compact and allow implementation of positive and negative inter-resonator couplings. A new class of microstrip slow-wave open-loop resonator filter was presented in [25]. The filters were not only compact, but also have a wide upper stopband. In [26], a dual-band BPF was developed for Global Positioning System (GPS) and Fixed Satellite (FS) applications. However, the electrical response for the other band was not perfectly, which causes more energy loss. A BPF design method for suppressing spurious responses in the stopband was discussed in [27]. In [28], compact multi-band and UWB-BPF based on coupled half wave resonators was proposed. In [29], a quadruple mode BPF was optimized to minimized size with common-via holes. In [30], an active band-pass R-filter output response at different values of center frequency was proposed.

However, the filter can not work well in the required frequency range, especially low frequencies. In [31], a design method for matching a frequency varying load to a lossless transmission line at N frequency points using N transmission line sections was discussed.

Split ring resonator (SRR) is an artificially produced structure, which could enhance the performance of BPFs [32-47]. For an individual SRR, as well as two-coupled SRRs, [32] theoretically observes strong resonances with high quality factors. In [33], applying an approach to improve SRR based BPF structure, the characteristics of the prototype has good agreements with design ones. The concept of complementary square split ring resonator (CSRR) was applied in [34], whose second harmonic frequency is suppressed. In [35], a set of SRR applies the concept of Wave Concept Iterative Procedure algorithm (WCIP) combining with the Multi-scale approach's module (MWCIP), which solves relationship between circuit complexity and computation time. In [36], in order to reduce to size the filter, broad side-coupled microstrip BPFs on multilayer substrates were employed. In [37], a full wave analysis was applied on the wideband BPF, whose CSRR is used as basic resonant unit. A dual-band BPF was generated and optimized in [38], which uses metamaterial SRRs. In [39], conventional SRR's characteristic of mixed couplings with the possible arrangements on one side was discussed. In [40], transmission characteristics of rectangular SRR with single and double splits were simulated and analyzed. In [41], a bandpass substrate CSRR based integrated waveguide (SIW) filter was simulated and analyzed, by implementing the SIW filter on the microstrip board, the insertion loss becomes –0.47dB. In [42], composite-right-left-handed transmission lines (CRLH) were employed on second- and third-order BPFs. A single cell unit CSRR and Chebyshev BPF ware simulated and analyzed in [43]. In [44], a six-pole of cascade microstrip BPF was designed with SRR. In [45, 46], a coplanar CPW loaded with SRRs were implemented for novel sensing devices. Based on radio-frequency microelectromechanical system (RF-MEMS), the SRR switches were considered as: (i) bridge type RF-MEMS with CSRRs; (ii) cantilever-type RF-MEMS with SRRs; (iii) cantilever-type RF-MEMS integrated with SRRs. In [47], a microstrip bandstop filter based on square SRRs was simulated on LPFs and BSFs.

Superformula is a generalization of the superellipse which was proposed by Jphan Gielis twenty years ago. The purpose of superformula generation was to describe complex shapes and curves found in nature. The mathematic function was also explained in [48]. After fifteen years of superformula generated, a simplified mathematic method to draw natural nonlinear

modifications of superformula was discussed in [49]. Because of their importance in figure generation, superformula used in SRR has been investigated and studied in the literature [50-52]. In [50], an effective technique of replacing the conventional circular rings with superformula shapes was employed in BPF design, which 21.3% reduction in the physical area and achieving acceptable responses. In [51], a design of high-performance microwave component was implemented in CSRR based on Gielis transformation.

1.5 Thesis Outline

Chapter 2 describes NTL technique, which could reduce the length of transmission line (TL) when building a LPF. The technique is employed on the stepped impedance LPFs in two paths, which are 2 dimensions (width of NTL) and 3 dimensions (thickness, width and height of the substrate). First, the interpretations of NTLs will be introduced. After that, the 2D and 3D applied optimization procedure will be discussed in sequence. To validate the optimization procedure, all optimized designs are simulated by full-wave simulators. At the end of this chapter, the comparable simulation results are also listed and explained.

Chapter 3 is about the superformula shape implemented on SRRs achieving a reduced area of microwave BPFs. All miniaturized SRR-BPFs (single-, dual-, and triple-order) are simulated using full-wave simulators.

Chapter 4 concludes the thesis, and suggests several possible future works.

CHAPTER 2. NON-UNIFORM TRANSMISSION LINES BASED LOWPASS FILTER DESIGNS

Nowadays, obtaining compact microwave components is one of the main topics of microwave engineering. Researchers have been proposing new designs and implementing theories to minimize the physical area, such as split ring resonator (SRR), defected ground structure (DGS), and multi-layer layouts. Under this background, this chapter will present compact LPF designs using two types of optimized NTLs: 2- and 3-dimensions.

2.1 2D NTLs based LPF

In this section, 2-dimention optimized LPFs are presented. The purpose of using NTLs are to get same (or better) electrical characteristics as compared to conventional designs without compromising area, electrical performance, and design complexity.

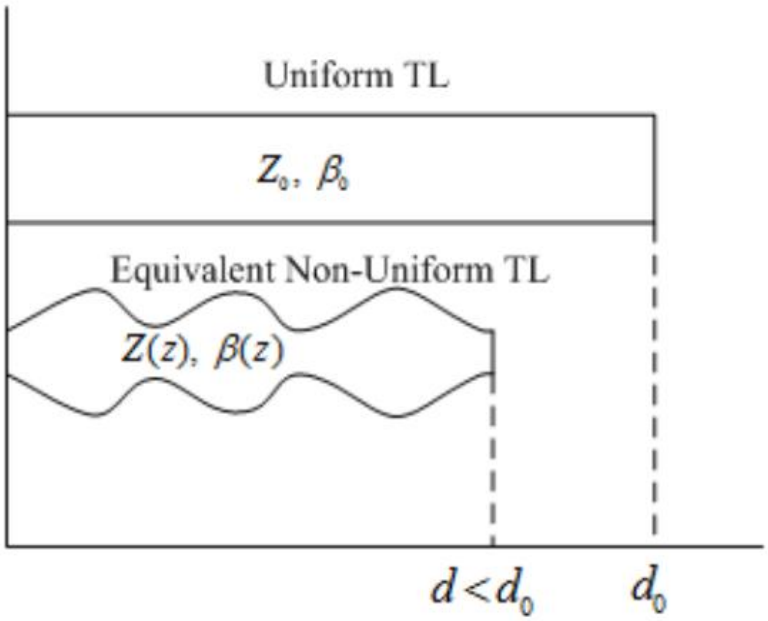

Figure 2.1. NTL Compared with UTL [21]

Figure 2.1. shows the main objective of using NTLs, which is the reduction of length. Also, it shows design parameters such as length d_0, characteristic impedance Z_0, and propagation constant β_0. In an equivalent NTL, the parameters that need to be considered are physical length d, varying characteristic impedance $Z(z)$, and propagation constant $\beta(z)$.

2.1.1 Mathematical Methodology

First, the effective dielectric constant ε_e is described in [52], which is also given as follows:

$$\varepsilon_e = \frac{\varepsilon_r + 1}{2} + \frac{\varepsilon_r - 1}{2} \cdot \frac{1}{\sqrt{1 + \frac{12h}{W}}} \tag{2.1}$$

where ε_r is dielectric constant, h stands for the thickness of the substrate, and W stands for the width of transmission line. The characteristic impedance Z_0 is:

$$Z_0 = \begin{cases} \dfrac{60 \ln(\frac{8h}{W} + \frac{W}{4h})}{\sqrt{\varepsilon_e}}, & \dfrac{W}{h} < 1 \\ \dfrac{120\pi}{\sqrt{\varepsilon_e}[\frac{W}{h} + 1.393 + 0.667 \ln(\frac{W}{h} + 1.444)]}, & \dfrac{W}{h} > 1 \end{cases} \tag{2.2}$$

By using equation (2.1) and (2.2), W can be defined under either of the conditions:

$$\frac{W}{h} = \begin{cases} \dfrac{8e^A}{e^{2A} - 2}, & \dfrac{W}{h} < 2 \\ \dfrac{2}{\pi}\left[B - 1 - \ln(2B - 1) + \dfrac{\varepsilon_r - 1}{2\varepsilon_r}\left\{ \ln(B - 1) + 0.39 - \dfrac{0.61}{\varepsilon_r} \right\} \right], & \dfrac{W}{h} > 2 \end{cases} \tag{2.3}$$

where A and B are constants. A is considered as:

$$A = \frac{Z_0}{60} \sqrt{\frac{\varepsilon_r + 1}{2} + \frac{\varepsilon_r - 1}{\varepsilon_r + 1}(0.23 + \frac{0.61}{\varepsilon_r})} \tag{2.4}$$

and B is given as follows:

$$B = \frac{377\pi}{2Z_0\sqrt{\varepsilon_r}} \tag{2.5}$$

The design of NTLs starts by dividing d into K short sections where the length of each section Δz is given as:

$$\triangle z = \frac{d}{K} \ll \lambda = \frac{c}{f} \tag{2.6}$$

where c is the speed of light, λ is the wavelength, and f is the operation frequency. The overall $ABCD$ matrix of the NTL is obtained by multiplying the individual $ABCD$ matrix as follows:

$$\begin{bmatrix} A & B \\ C & D \end{bmatrix} = \begin{bmatrix} A_1 & B_1 \\ C_1 & D_1 \end{bmatrix} \cdots \begin{bmatrix} A_i & B_i \\ C_i & D_i \end{bmatrix} \cdots \begin{bmatrix} A_K & B_K \\ C_K & D_K \end{bmatrix} \tag{2.7}$$

where *ABCD* parameters of each section can be expressed as:

$$\begin{bmatrix} A_i & B_i \\ C_i & D_i \end{bmatrix} = \begin{bmatrix} \cos(\Delta\theta) & jZ_i \sin(\Delta\theta) \\ jZ_i^{-1} \sin(\Delta\theta) & \cos(\Delta\theta) \end{bmatrix} \tag{2.8}$$

Moreover, the electrical length of each part $\Delta\theta$ can be written as:

$$\Delta\theta = \frac{2\pi}{\lambda}\Delta z = \frac{2\pi}{c} f \sqrt{\varepsilon_e}\,\Delta z \tag{2.9}$$

In order to calculate the width of each section, truncated Fourier series formula for the normalized characteristic impedance $\overline{Z}(z) = Z(z)/Z_0$ is considered as follows:

$$\ln(\overline{Z}(z)) = a_0 + \sum_{n=1}^{N=5} (c_n \cos(\frac{2\pi nz}{d}) + b_n \sin(\frac{2\pi nz}{d})) \tag{2.10}$$

where a_0, b_n, and c_n are Fourier coefficients. To obtain the LPF response, the optimization procedure is carried out by minimizing the following error function:

$$E = \sqrt{\frac{1}{N_f}\left(\left(|S_{11}|^2 + \left(|S_{21}| - |S_{21}|_{desired}\right)^2\right)_{0 \le f \le f_c} + \left(\left(|S_{21}| - |S_{21}|_{desired}\right)^2\right)_{f_c \le f \le f_m}\right)} \tag{2.11}$$

where S_{11} is input port matching and S_{21} is the transmission parameter of the NTL, f_c is the cutoff frequency, and N_f is the number of the frequency points in the range of [*0*, f_m]. The S-parameters could be found by the following equations:

$$S_{11} = \frac{AZ + B - CZ^2 - DZ}{AZ + B + CZ^2 + DZ} \tag{2.12a}$$

$$S_{21} = \frac{2Z}{AZ + B + CZ^2 + DZ} \tag{2.12b}$$

Meanwhile, the error function (2.11) has to be minimized under some constraints, such as reasonable fabrication and physical matching:

$$W_{\min} \le W(z) \le W_{\max} \tag{2.13a}$$

$$Z(0)=Z(d)=50\Omega \tag{2.13b}$$

Since the width is related with the characteristic impedances in (2.2), the first constraint (2.13a) is to ensure that physical width of the NTL is within acceptable range by considering an

appropriate W_{max} and W_{min}. Meanwhile, the second constraint (2.13b) is for ensuring the normalized impedance of first section *Z(0)*, as well as the final section *Z(d)* are perfectly matched with the feedline. For both of constraints to be achieved, the sum of the Fourier coefficients should be zero.

2.1.2 Structural Designs

In this section, the physical and electrical parameters are presented. The purpose of this optimization is to find the best set of Fourier coefficients a_0, b_n, and c_n, which could offer the NTL a minimized optimization error. All of the coefficients should be chosen or designed under the constraints set (2.13) during the optimization. The minimum width of the NTL is chosen to be 0.1 mm and maximum width is chosen as 10 mm. According to the aforementioned equations, Z_{max}=135.5Ω and Z_{min}=13.5Ω. The NTL is implemented on Rogers RO4003C substrate with 0.813 mm thickness, whose relative permittivity ε_r is 3.55, with a dielectric loss (*tanδ*) of 0.0027.

Besides the constraints, other specifications need to be considered. The cutoff frequency f_c is set to 3.5 GHz, and the maximum frequency f_m is set to 6 GHz. The transmission loss in passband is set to 0 dB, while the transmission loss in stopband is set to –20 dB. The number of total sections *K* is set to 50, and as for the inputs of Fourier coefficients, they were bounded between 1 and –1. It is worth to mention that the MATLAB function 'fmincon' is used to solve the optimization problem.

Furthermore, in order to verify the analytical results generated in MATLAB, Ansys High Frequency Structure Simulation (HFSS) software is used for simulation. Firstly, the NTL is imported into AutoCad. Then, the DXF file is created in AutoCad and imported into HFSS to run simulation.

2.1.3 2D Design Results

2.1.3.1 Conventional Stepped Impedance LPF

Firstly, a conventional LPF is designed for comparison with the 2D modified design, Table 1 shows the impedance values and length values in the LPF, as presented in [52].

Table 1 Impedance and Lengths in LPF

Section	$Z(\Omega)$	$\beta l(rad)$	$W(mm)$	$d(mm)$
1	13.67	0.0853	9.981	1.2862
2	133.38	0.3404	0.198	5.8866
3	13.67	0.3866	9.981	5.8194
4	133.38	0.668	0.198	11.553
5	13.67	0.5401	9.981	8.1204
6	133.38	0.7405	0.198	12.8068
7	13.67	0.4872	9.981	7.3254
8	133.38	0.5301	0.198	9.1684
9	13.67	0.2482	9.981	3.7326
10	133.38	0.1173	0.198	2.0286

Then, the physical parameters are incorporated into HFSS. Figure 2.2. shows the structure of conventional stepped impedance LPF. The maximum and minimum width values are 9.981 mm and 0.198 mm, and the total length is 67.7274 mm.

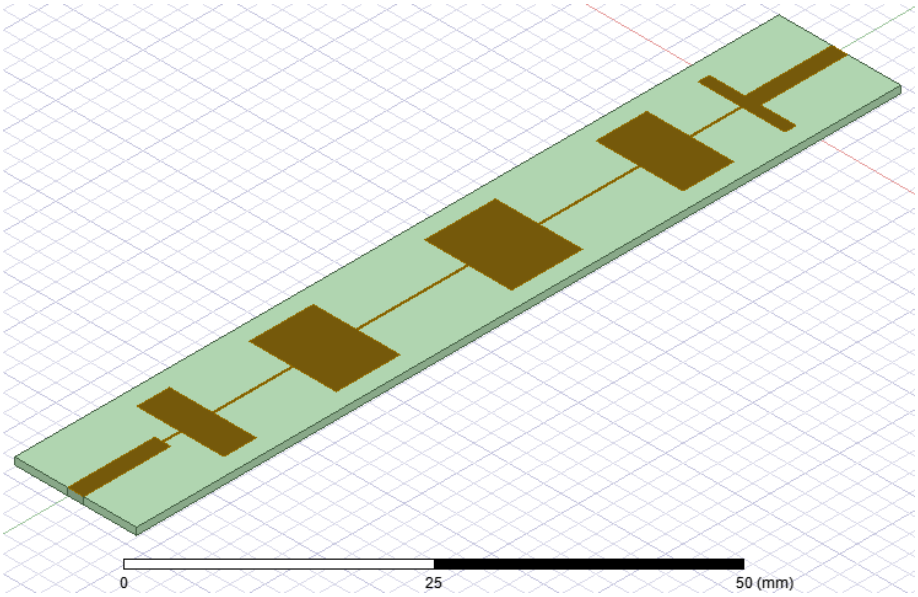

Figure 2.2. Conventional Stepped Impedance LPF Structure with f_c = 3.5 GHz

Figure 2.3. shows the conventional stepped impedance LPF S-parameters with f_c =3.5 GHz. S_{11} in passband is better than –12 dB within [0 3.5] GHz. S_{21} is better than –58 dB when f_m =6 GHz, whereas S_{11} is 0 dB meaning signals are fully filtered out in stopband.

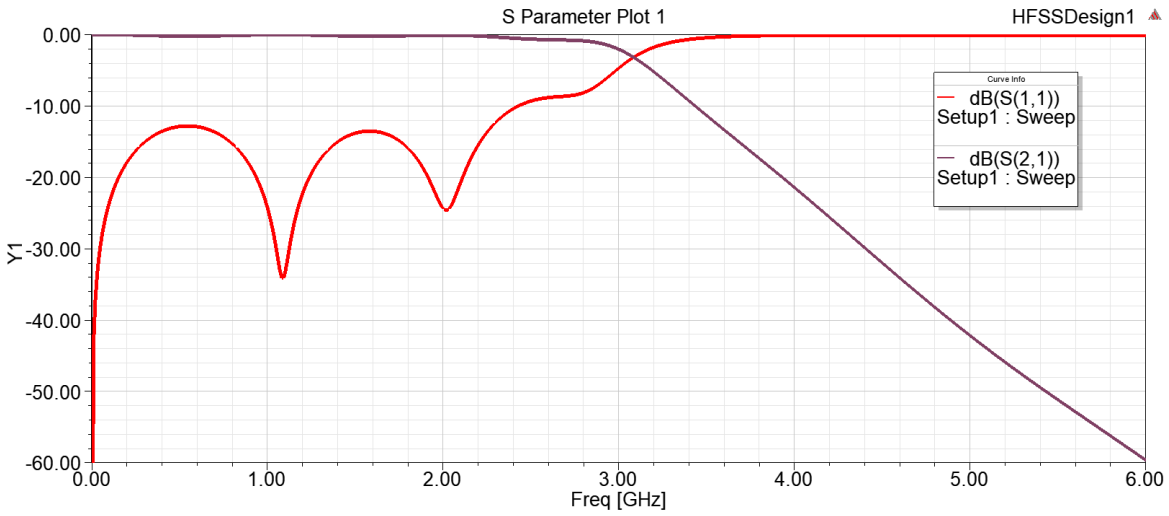

Figure 2.3. Conventional Stepped Impedance LPF S-parameters with f_c = 3.5 GHz

2.1.3.2 2D-NTL Design

Figure 2.4. shows the analytical result of S_{11} and S_{21} of the NTL-LPF. S_{11} is better than –15 dB with in [0 f_c] GHz passband, and S_{21} is better than –43 dB when f_m = 6 GHz.

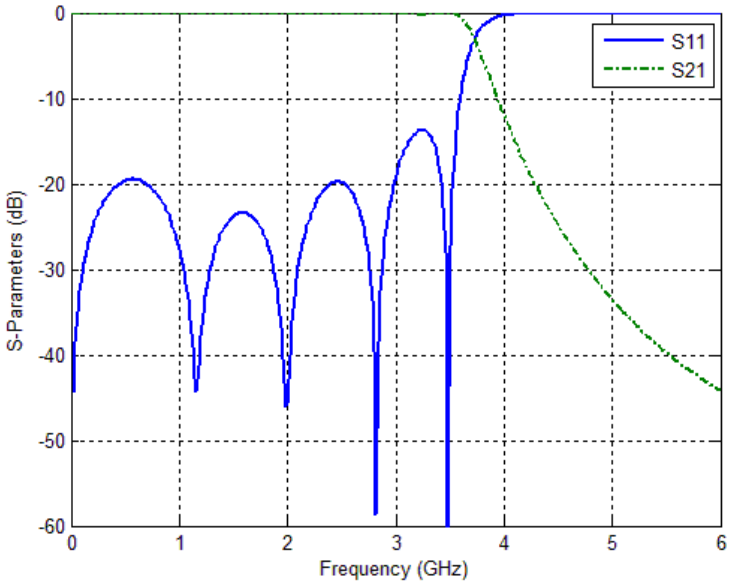

Figure 2.4 S-parameter of 2D-modified Design

In Figure 2.5., the NTL filter is showing the minimum width of the LPF trace is 0.18558 mm; whereas the maximum width is 8.8 mm. The physical parameters follow in constraints as expected.

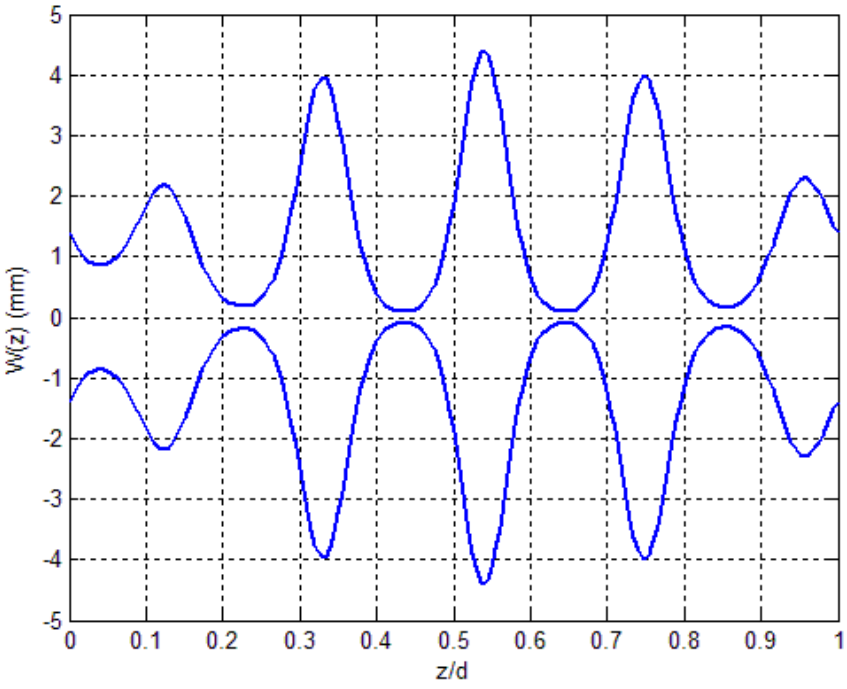

Figure 2.5. Width-Variation of 2D-modified LPF

Furthermore, the optimized Fourier series coefficients of 2D-NTL design are provided in Table 2, where the error function error is 0.0651.

Table 2 Coefficients of Fourier Series Design

a_0	c_1	b_1	c_2	b_2	c_3	b_3	c_4	b_4	c_5	b_5
–0.096	–0.03	–0.01	–0.056	–0.1	–0.11	–0.09	–0.23	–0.33	0.252	0.745
E = 0.0651										

In order to verify the analytical results, Ansys HFSS is used to simulate and justify the NTL design. Figure 2.6 shows the simulated structure.

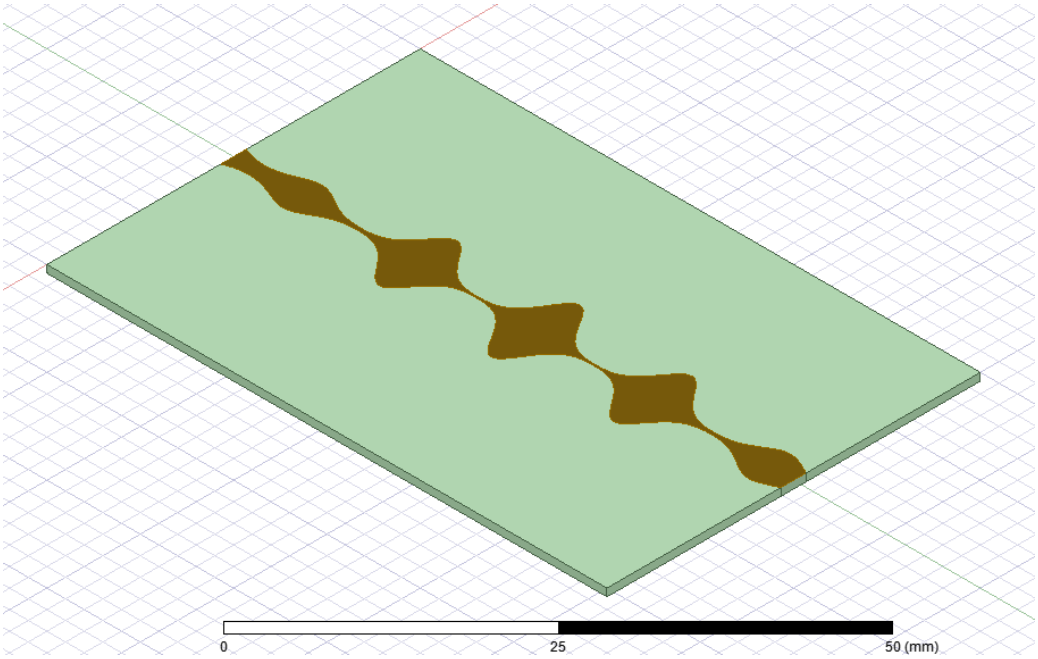

Figure 2.6. Structure of the 2D-Modified LPF

Figure 2.7. shows the S-parameters of the 2D NTL-LPF simulation. S_{11} is better than –12 dB within [0 3.5] GHz passband. S_{21} is better than –40 dB when f_m =6 GHz. Hence, the simulation results meet the requirement.

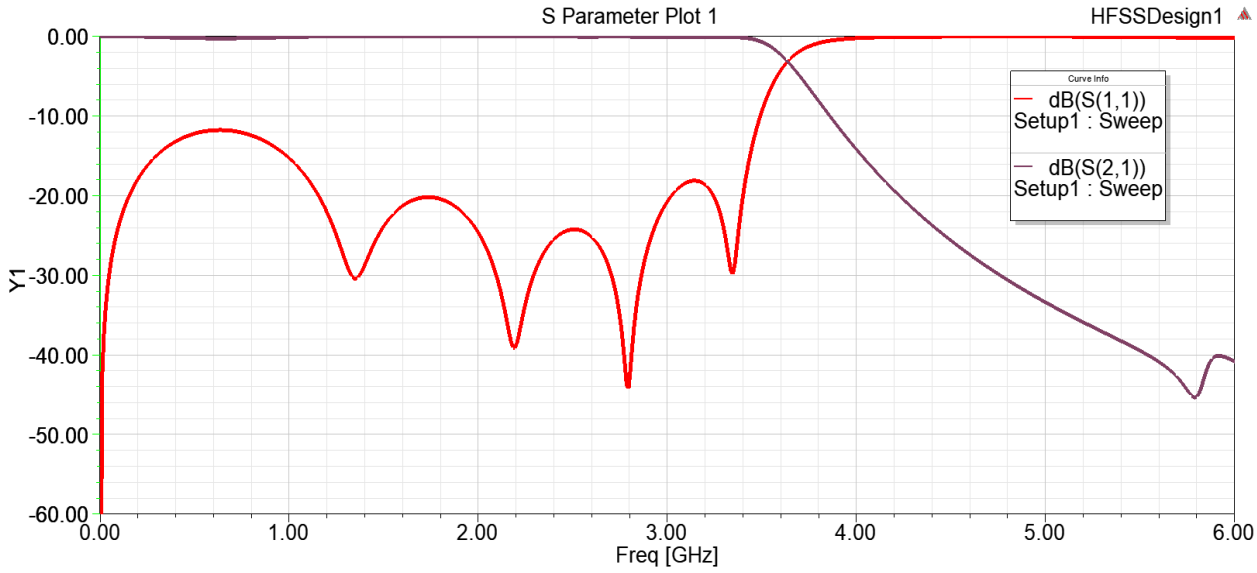

Figure 2.7. Simulation Results of the LPF

Figure 2.8. shows the comparison result of the conventional stepped impedance LPF design and the 2D optimized design.

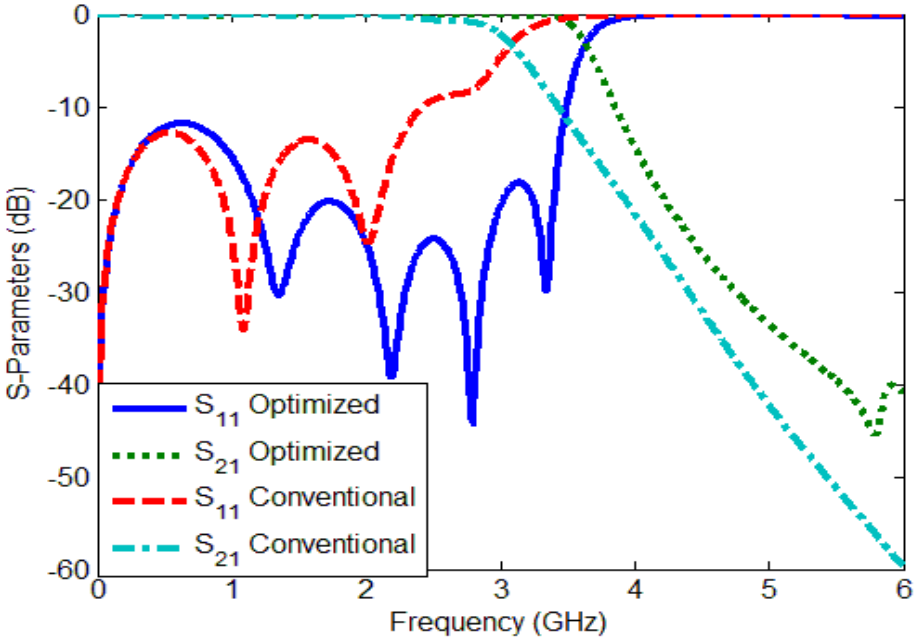

Figure 2.8. Comparison Results of the LPFs

Table 3 shows the comparison result of the conventional stepped impedance LPF design and the 2D optimized design, where 'S_{11}(dB)' stands for S_{11} in passband. Hence, by keeping the same electrical responses, the 2D optimized design is 12.83% shorter than the conventional stepped impedance LPF design.

Table 3 Comparison of Conventional/2D-NTL based LPF

	S_{11}(dB)	Length(mm)
Conventional UTL-LPF	–13	67.24
Width-Modified NTL-LPF	–13	60
Comparison	0	12.83%

2.1.3.3 Comparison results

For comparison, NTL based LPFs with different lengths are analyzed. Figure 2.9. and Figure 2.10. show the electrical response and the NTL trace when d = 80mm:

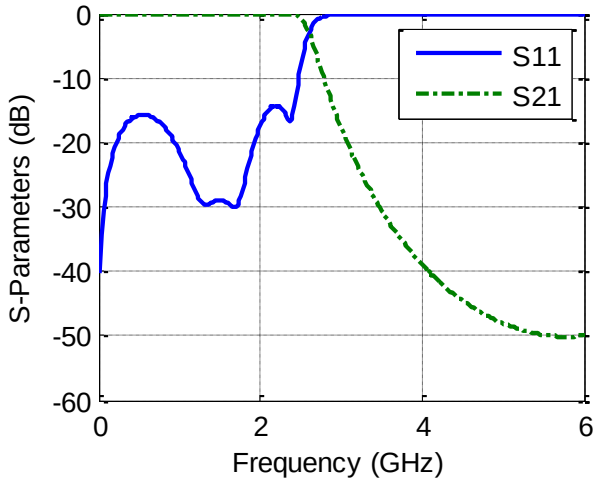

Figure 2.9. S-parameters when d = 80mm

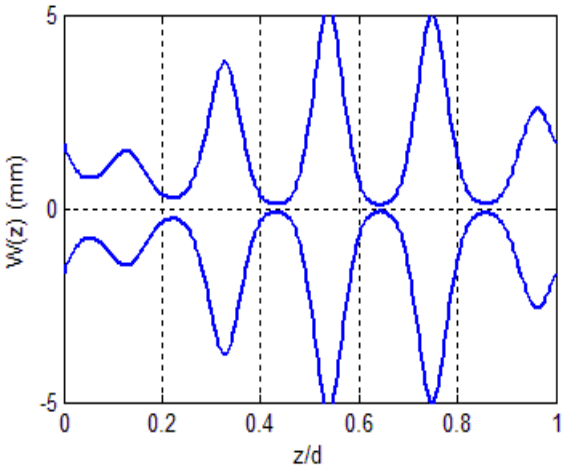

Figure 2.10. Designed Trace when d = 80mm

Table 4 shows coefficients of Fourier series for 80 mm length, where the error function is 0.2310.

Table 4 Coefficients of Fourier Series for 80 mm Length by 2D-Optimized

a_0	c_1	b_1	c_2	b_2	c_3	b_3	c_4	b_4	c_5	b_5
–0.11	0.03	0.041	–0.03	–0.015	–0.12	–0.04	–0.38	–0.32	0.22	0.74
E = 0.2310										

Figure 2.11. and Figure 2.12. show the electrical response and the NTL trace when d = 100mm:

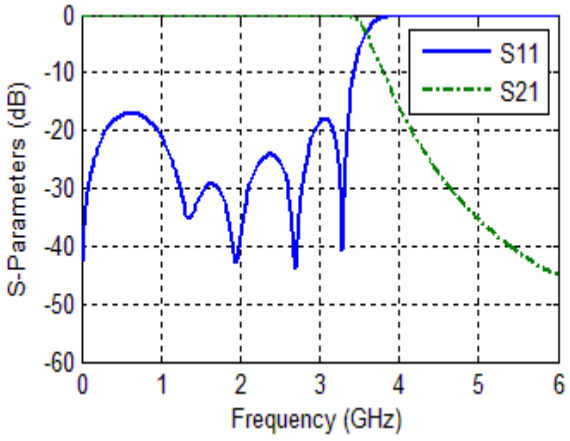

Figure 2.11. S-parameters when d = 100mm

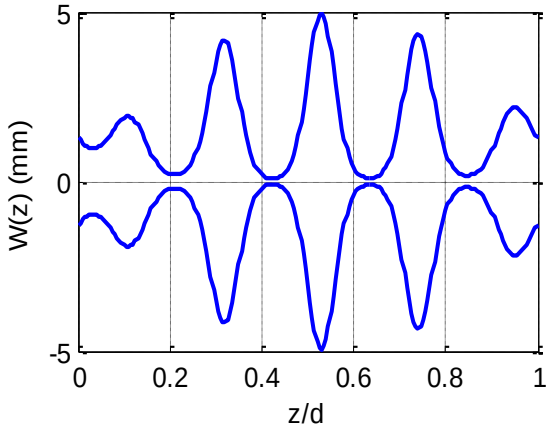

Figure 2.12. Trace when d = 100mm

Table 5 shows coefficients of Fourier series for 100 mm length, where the error function result is 0.0519.

Table 5 Coefficients of Fourier Series for 100 mm Length by 2D-Optimized

a_0	c_1	b_1	c_2	b_2	c_3	b_3	c_4	b_4	c_5	b_5
–0.12	–0.01	0.011	–0.05	–0.016	–0.13	–0.06	–0.38	–0.33	0.458	0.6076
E = 0.0519										

Figure 2.13 and Figure 2.14 show the electrical response and the NTL trace when d = 120mm:

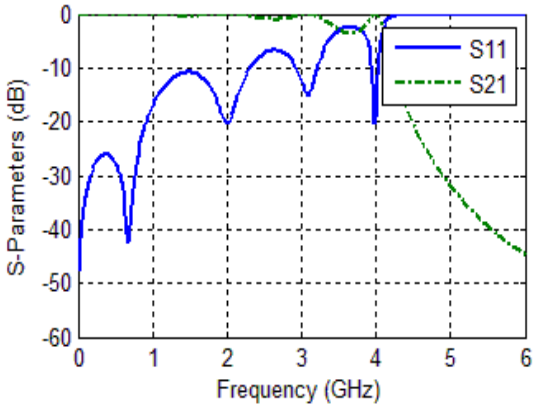

Figure 2.13. S-parameters when d = 120mm

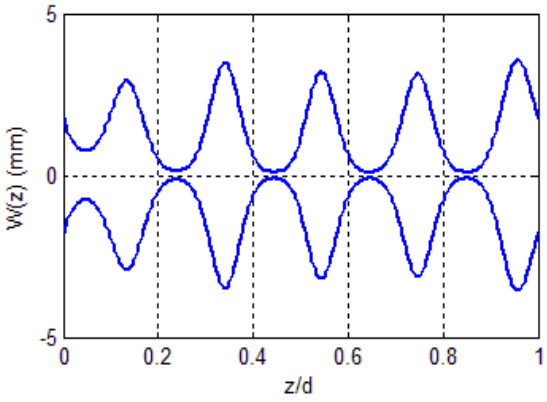

Figure 2.14. Designed Trace when d = 120mm

Table 6 shows coefficients of Fourier series *f*or 120 mm length, where the error function result is 0.3001:

Table 6 Coefficients of Fourier Series for 120 mm Length by 2D-Optimized

a_0	c_1	b_1	c_2	b_2	c_3	b_3	c_4	b_4	c_5	b_5
–0.06	–0.15	–0.06	–0.13	–0.053	–0.14	–0.08	–0.11	–0.16	0.1567	0.8312
E = 0.3001										

As compared, this group of result is not acceptable. The electrical and physical requirements are best met when 60 mm length is used.

2.2 3D NTL Structure

In this section, 3-dimension optimized NTLs are presented. Besides the width variation, the thickness of the substrate, as well as length of NTL is varied in the optimization procedure. In this section, the thickness of the substrate is set as an optimized variable, rather than fixed one. Length modification is set as an optimized variable later on.

2.2.1 Mathematical Methodology

This design is based on the 2D modified NTL design. In (2.10), the width of each section is varied by applying Fourier series. Here, the thickness modeled in another Fourier series. The thickness $\overline{H}(z)$ is given as follows:

$$\ln(\overline{H}(z)) = a_1 + \sum_{n=6}^{N=10} (c_n \cos(\frac{2\pi nz}{d}) + b_n \sin(\frac{2\pi nz}{d})) \tag{2.14}$$

where a_1, c_n and b_n are Fourier series variables bounded between two and negative two.

2.2.2 Structural Design

In this section, the constraints of the non-uniform transmission lines (NTLs) are still valid, which means the width of NTL is varied between 0.2 mm and 10 mm. Additionally, the thickness of the substrate based on the physical limitation is in the range [0.1 3] mm. For this design, the NTL is also going to be implemented on Rogers RO4003 substrate, whose relative permittivity ε_r is 3.55, with a dielectric loss (*tanδ*) of 0.0027. For the optimized length and width structure, $Z_0 = Z(d) = 50\ \Omega$.

This 3D NTL design is considered to build a LPF with a cutoff frequency 2 GHz, and the maximum frequency is set to 6 GHz. The transmission loss in passband is set to 0 dB, while the stopband loss is set to –20 dB. The Fourier coefficients were bounded between 2 and –2. In the first part, 60 mm NTL length is employed in the design. In the second part, the length is optimized considering a range of [35 45] mm.

The purpose of the optimized *d* is to minimize the length of NTL, and get the same or better results compared with the conventional design. ‘fmincon’ function is used to optimize the error function. Meanwhile, different error weight is applied to obtain better responses.

Furthermore, in order to validate the analytical results, Ansys HFSS is used for simulation. Firstly, the physical parameters generated in MATLAB are imported into AutoCad. Then, the DXF file, as well as SAT file is imported to HFSS to run simulations.

2.2.3 Result of 3D NTL Modified Layout

The main objective of this design is gaining the same or better propagation responses with a reduced length. Firstly, conventional stepped impedance LPF is designed and simulated. Secondly, the process of 3D NTL-LPF optimization with d = 60 mm is carried out. Last but not least, a length- , thickness, and width-modified 3D NTL-LPF design is presented.

2.2.3.1 Conventional Stepped Impedance LPF

Firstly, a conventional LPF with a 2 GHz cutoff frequency is built.

Table 7 Impedance values and Corresponding Length Values of LPF

Section	$Z(\Omega)$	$\beta d(rad)$	$W(mm)$	$d(mm)$
1	13.65	0.1411	9.876	3.7172
2	133.35	0.5302	0.1752	16.0428
3	13.65	0.5274	9.876	13.8782
4	133.35	0.3465	0.1752	21.9244
5	13.65	0.3860	9.876	10.1572
6	133.35	0.1939	0.1752	5.867

Table 7 illustrates the impedance values and corresponding length values of LPF.

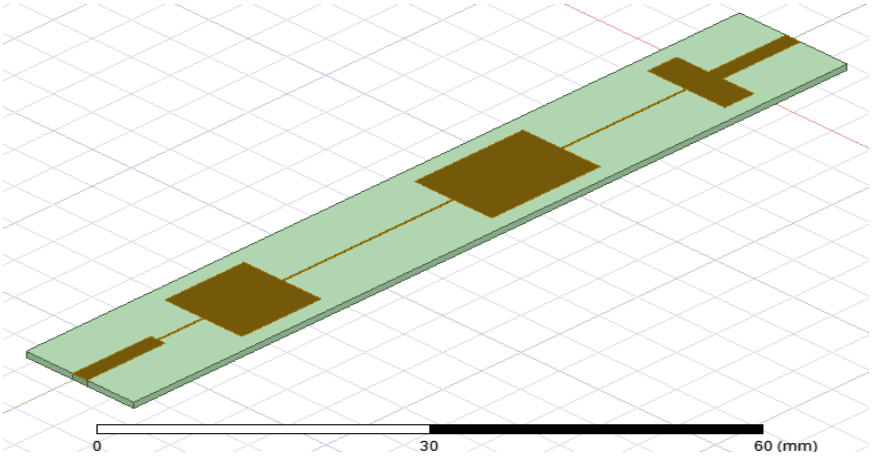

Figure 2.15. Structure of Conventional Stepped Impedance LPF in HFSS

The physical parameters are imported into HFSS software, which shows in Figure 2.15. Based on the Table 7, the total length of the conventional LPF design is 71.58 mm. Figure 2.16. shows the electrical response, S_{11} is better than –13 dB within [0 2] GHz passband. S_{21} is better than –40 dB when f_m = 6 GHz.

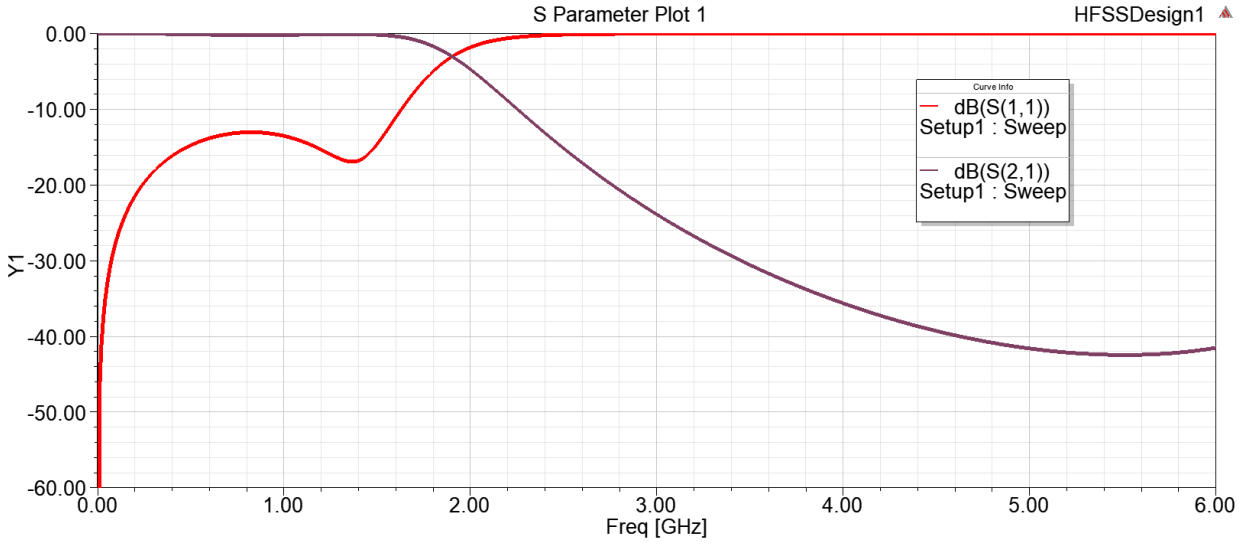

Figure 2.16. Simulation Results of Conventional Design in HFSS

2.2.3.2 3D NTL Design when Length

The analytical results of 60 mm length 3D NTL-LPFs is shown in Figure 2.17.:

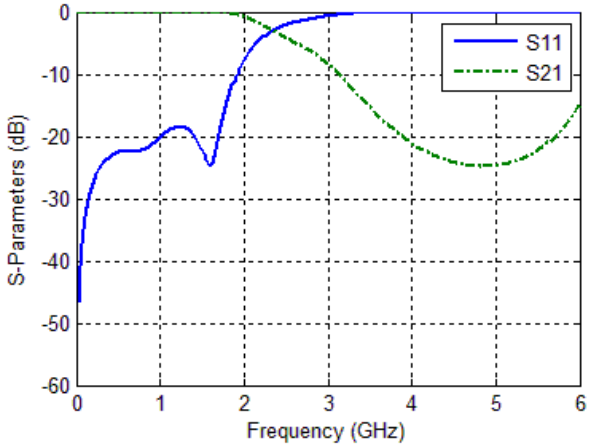

Figure 2.17. S-parameters when d = 60mm

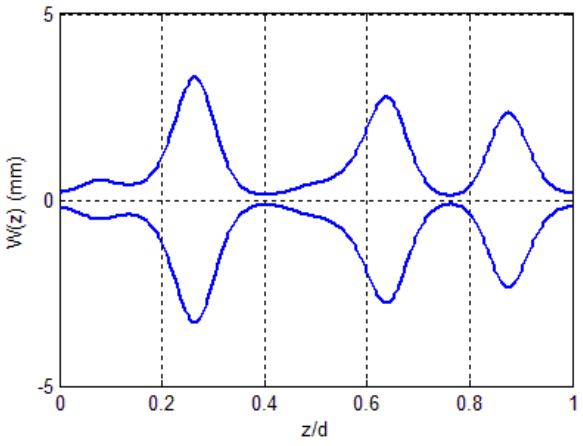

Figure 2.18. Width-Variation when d = 60mm

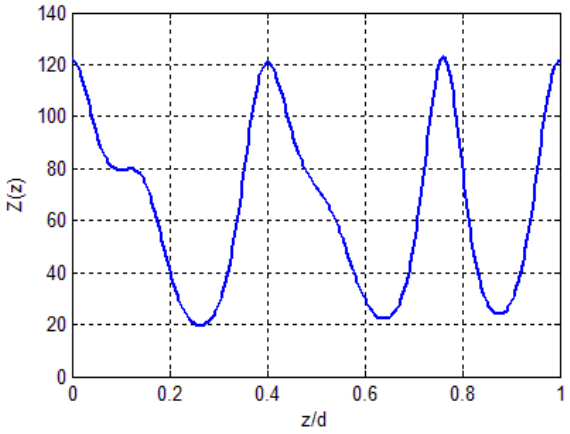

Figure 2.19. *Z*-Variation when *d* = 60mm

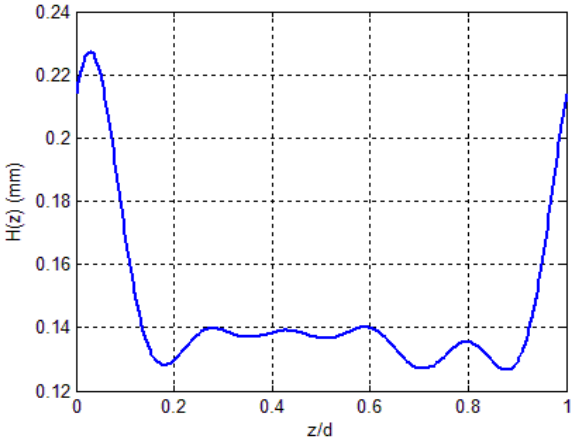

Figure 2.20. *H*-Variation when *d* = 60mm

Figure 2.16. is showing that S_{11} is better than –12 dB within [0 2] GHz passband. S_{21} is better than –40 dB when f_m=6 GHz, where S_{11} is 0 in stopband indicating excellent filtering.

Figure 2.17. shows the width-variation of 3D NTL design; Figure 2.18. is the optimized impedance of transmission line; Figure 2.19. shows optimized thickness of the substrate. The resulting Fourier series are indicated in Table 8:

Table 8 Coefficients of Fourier Series for 60 mm length by 3D-Optimized

Fourier Series for *Z*										
a_0	c_1	b_1	c_2	b_2	c_3	b_3	c_4	b_4	c_5	b_5
–0.06	–0.15	–0.06	–0.13	–0.053	–0.147	–0.086	–0.113	–0.16	0.156	0.83
Fourier Series for *H*										
a_1	c_6	b_6	c_7	b_7	c_8	b_8	c_9	b_9	c_{10}	b_{10}
–0.07	0.189	0.039	0.120	0.038	0.0829	0.0443	0.0507	0.059	0.018	0.03
E = 0.2416										

In this design, the error value is 0.241606. The minimum width is 0.24 mm, the maximum width is 0.548 mm; the maximum thickness is 2.27 mm, the minimum thickness is 0.13 mm; so the

physical parameters are also meeting the requirements. In order to validate the analytical result, a full-wave simulation has been run. The structure construction is showing in Figure 2.21.

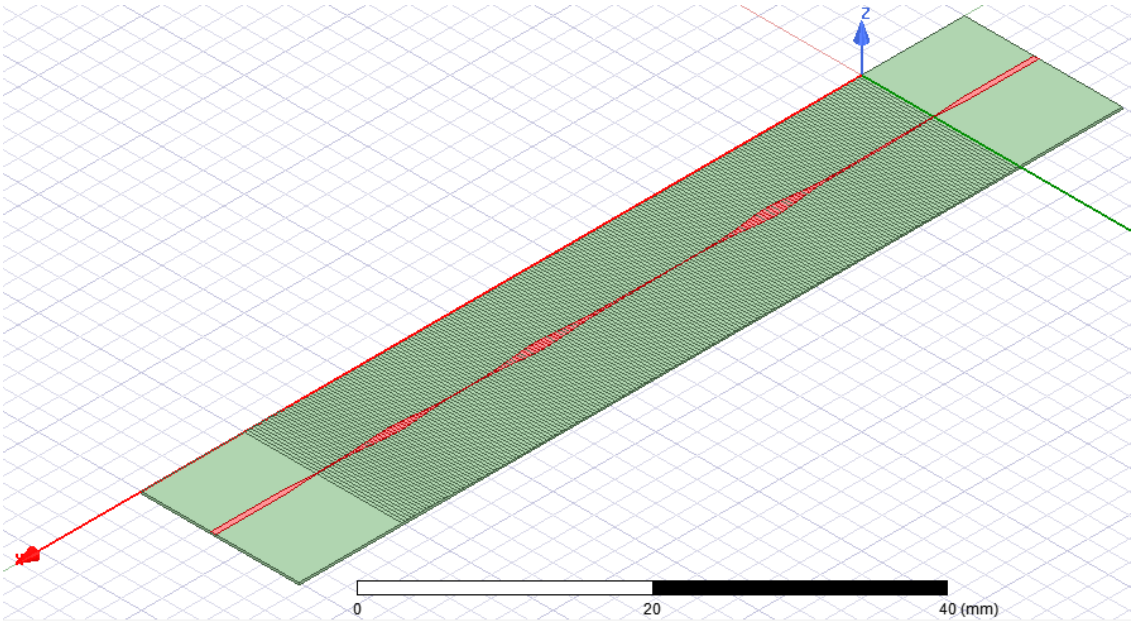

Figure 2.21. Structure of HFSS when d = 60 mm

Figure 2.22. shows electrical response of width- and thickness-modified NTL, where in passband, S_{11} is better than –15 dB, and in stopband, S_{21} is –15 dB when f_m = 6 GHz, which means the signal is filtered out.

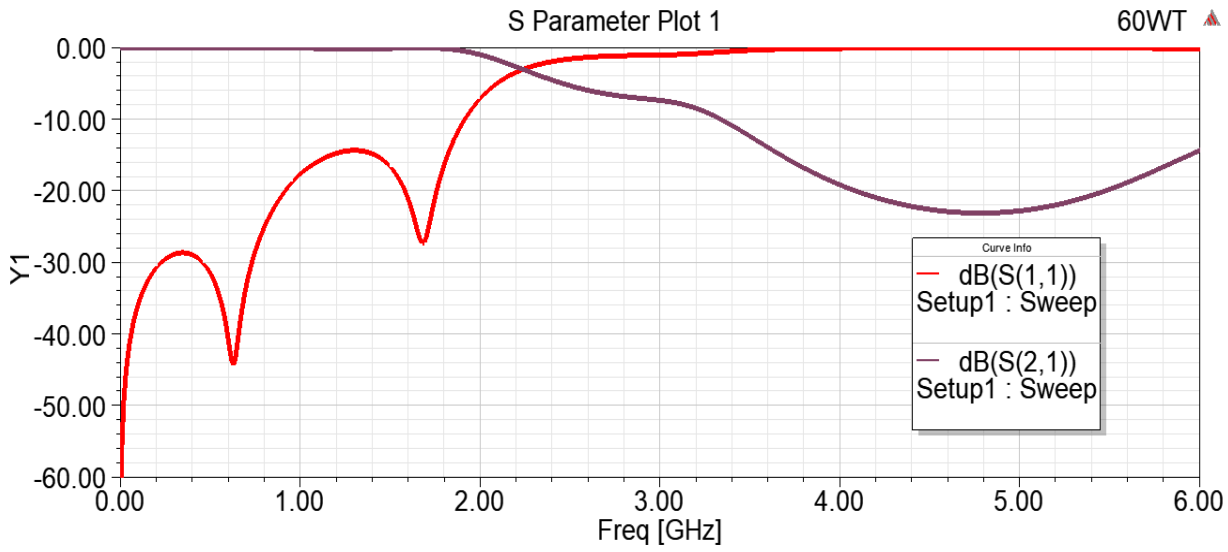

Figure 2.22. Simulation Result when d = 60 mm

Figure 2.23. shows the comparison result of the conventional LPF design and the 3D optimized design.

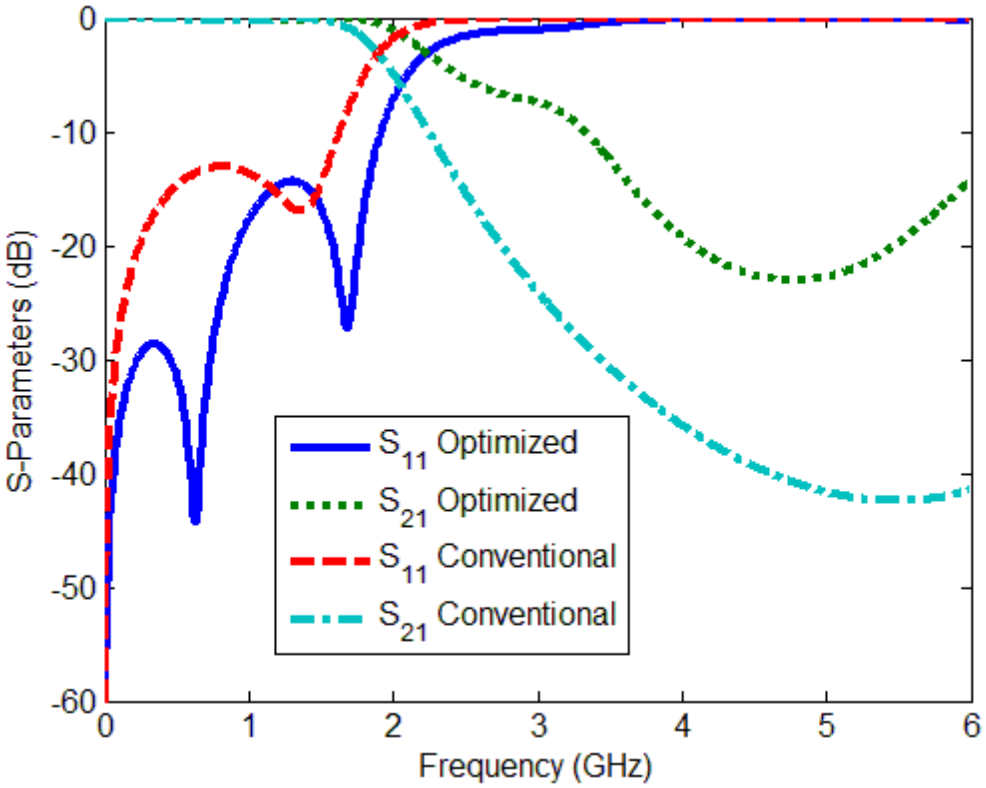

Figure 2.23. 3D-Modified Results when d = 60 mm

Table 9 shows the comparison result of the conventional LPF design and the 3D optimized design. Hence, by gaining 2dB better of S_{11} value in passband, the 3D optimized design is 19.3% shorter than the conventional stepped impedance LPF design.

Table 9 Comparison of Conventional/3D-Modified-NTL based LPF

	S_{11}(dB)	Length(mm)
Conventional UTL-LPF	–13	71.58
Width- and Thickness-Modified NTL-LPF	–15	60
Comparison	2	19.30%

2.2.3.3 3D NTL Design Results with Different Lengths

For comparison, NTL based LPFs with different lengths are analyzed. The cutoff frequency is 2 GHz, and the max of frequency is 6 GHz. The length of the comparable NTLs are set to 70mm; 80 mm; 100 mm; 120 mm. The results of 70 mm optimized design are showing as follows:

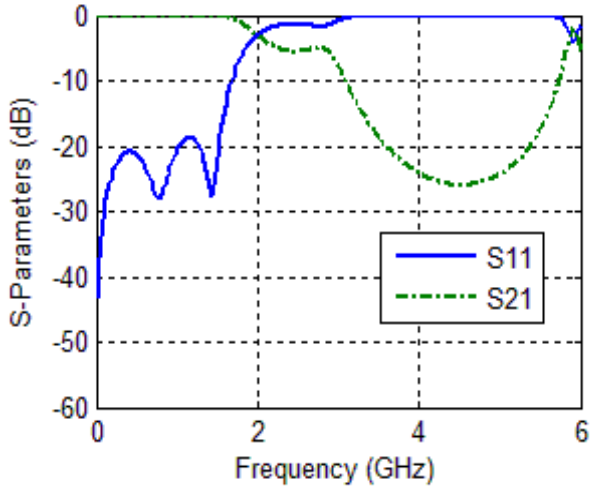

Figure 2.24. S-parameters when *d* = 70mm

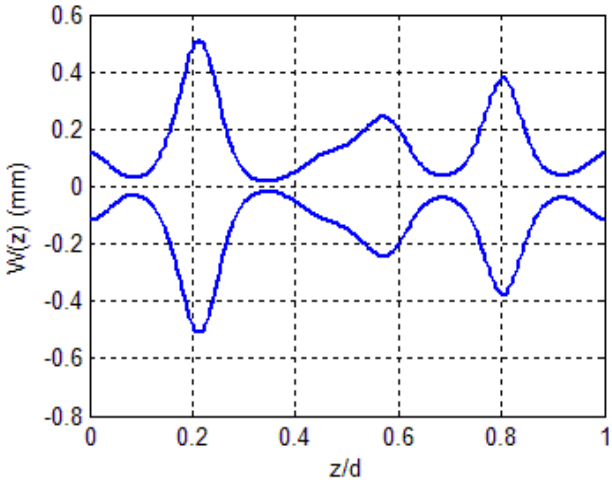

Figure 2.25. Width-Variation when *d* = 70mm

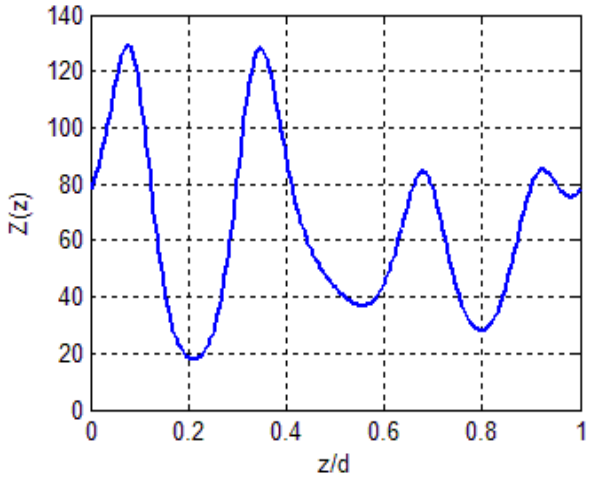

Figure 2.26. *Z*-Variation when *d* = 70mm

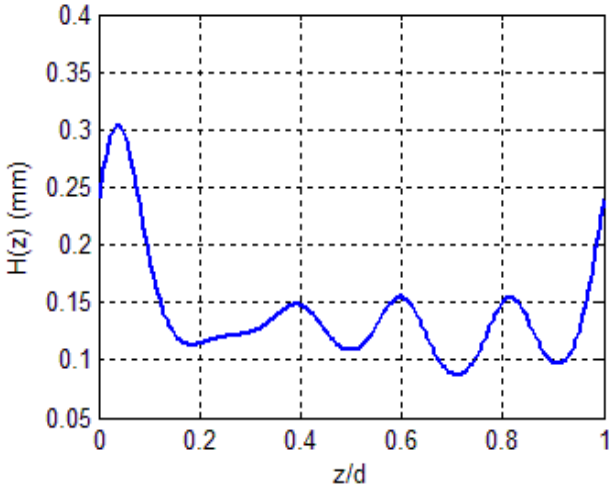

Figure 2.27. *H*-Variation when *d* = 70mm

Table 10 shows coefficients of Fourier series for 70 mm length, where the error function result is 0.279:

Table 10 Coefficients of Fourier Series for 70 mm Length by 3D-Optimized

Fourier Series for Z										
a_0	c_1	b_1	c_2	b_2	c_3	b_3	c_4	b_4	c_5	b_5
0.145	0.097	0.051	0.271	–0.115	0.473	0.243	–0.26	0.05	–0.3	–0.1
Fourier Series for H										
a_1	c_6	b_6	c_7	b_7	c_8	b_8	c_9	b_9	c_{10}	b_{10}
0.06	0.15	0.08	0.180	0.06	0.097	0.110	–0.04	0.202	0.14	0.1
E = 0.279										

The results of 80 mm optimized design are showing as follows:

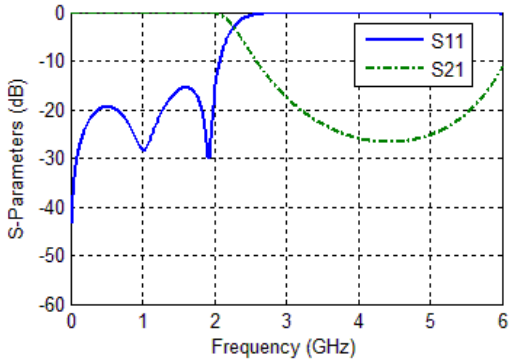

Figure 2.28. S-parameters when d = 80mm

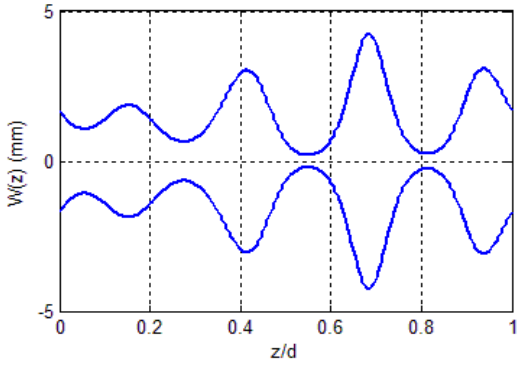

Figure 2.29. Width-Variation when d = 80mm

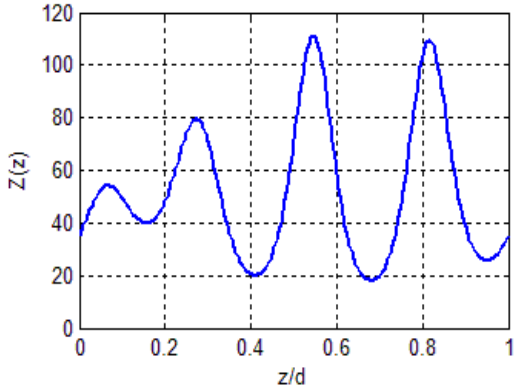

Figure 2.30. Z-Variation when d = 80mm

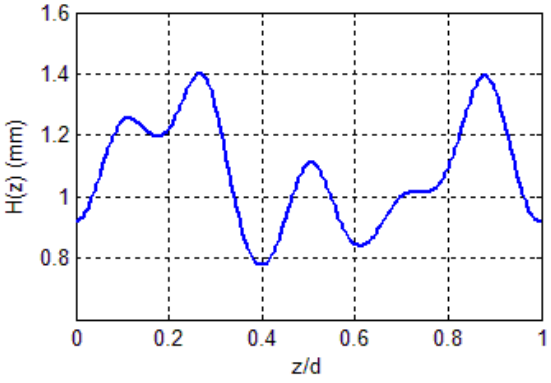

Figure 2.31. H-Variation when d = 80mm

Table 11 shows coefficients of Fourier series for 80 mm length, where the error function result is 0.0857:

Table 11 Coefficients of Fourier Series for 80 mm Length by 3D-Optimized

Fourier Series for Z										
a_0	c_1	b_1	c_2	b_2	c_3	b_3	c_4	b_4	c_5	b_5
–0.09	2.01	0.002	–0.08	0.0091	–0.37	–0.213	0.173	0.540	0.018	0.01
Fourier Series for H										
a_1	c_6	b_6	c_7	b_7	c_8	b_8	c_9	b_9	c_{10}	b_{10}
0.06	0.11	0.05	–0.07	–0.02	–0.101	–0.07	0.021	0.028	–0.10	0.02
E = 0.279										

The results of 100 mm optimized design are showing as follows:

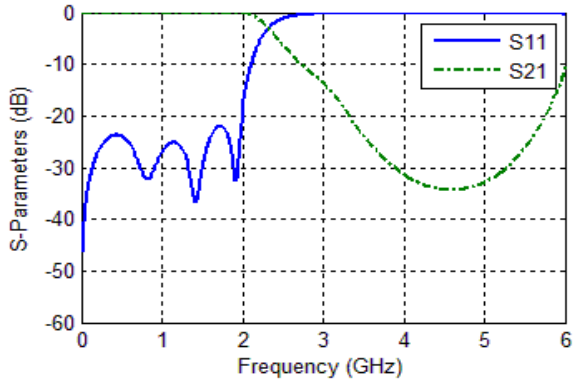

Figure 2.32. S-parameters when d = 100mm

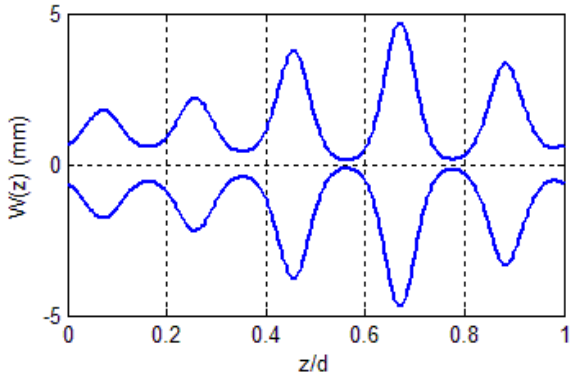

Figure 2.33. W-Variation when d = 100mm

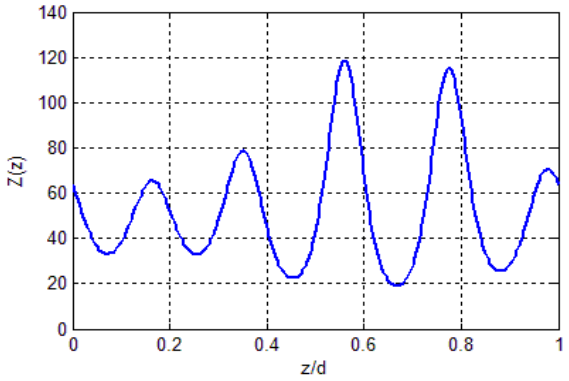

Figure 2.34. Z-Variation when d = 100mm

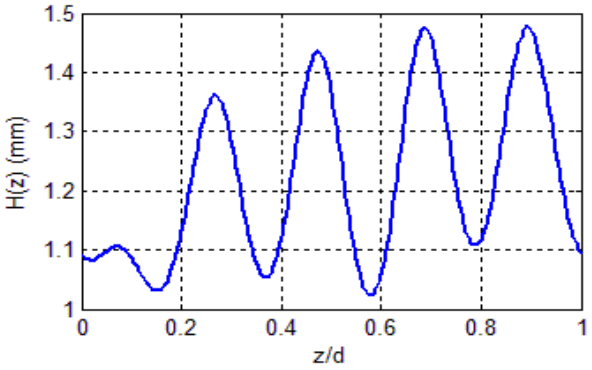

Figure 2.35.H-Variation when d = 100mm

The coefficients of Fourier series of 100 mm optimized design are showing as follows:

Table 12 Coefficients of Fourier Series for 100 mm Length by 3D-Optimized

Fourier Series for Z										
a_0	c_1	b_1	c_2	b_2	c_3	b_3	c_4	b_4	c_5	b_5
–0.05	–0.1	–0.02	–0.02	0.009	–0.06	–0.02	0.123	0.3	0.26	–0.5
Fourier Series for H										
a_1	c_6	b_6	c_7	b_7	c_8	b_8	c_9	b_9	c_{10}	b_{10}
–0.01	–0.5	–0.01	–0.05	0.004	–0.03	0.03	–0.06	–0.1	0.07	–0.5
E = 0.115118										

The results of 120 mm optimized design are showing as follows:

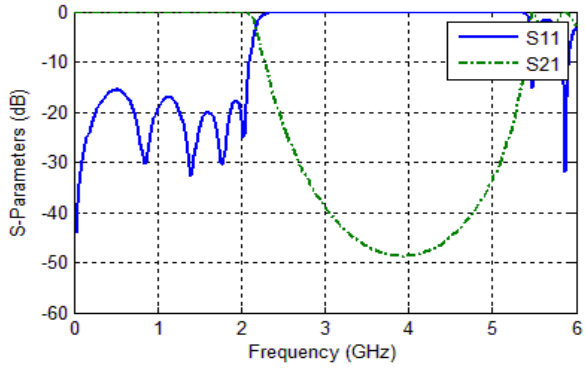

Figure 2.36. S-parameters when d = 120mm

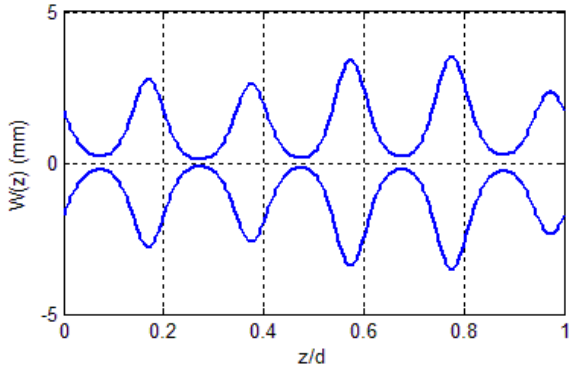

Figure 2.37. W-Variation when d = 120mm

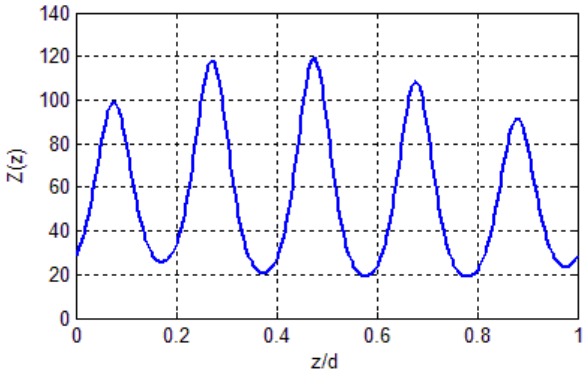

Figure 2.38. Z-Variation when d = 120mm

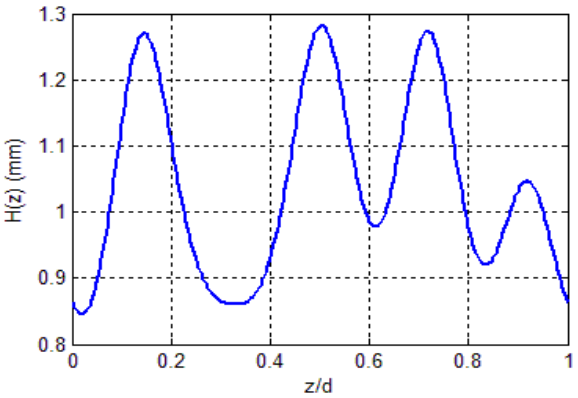

Figure 2.39. H-Variation when d = 120mm

The coefficients of Fourier series of 120 mm optimized design are showing in Table 13:

Table 13 Coefficients of Fourier Series for 120 mm Length by 3D-Optimized

Fourier Series for Z										
a_0	c_1	b_1	c_2	b_2	c_3	b_3	c_4	b_4	c_5	b_5
–0.04	–0.7	0.09	–0.01	0.031	0.001	–0.017	0.068	–0.09	–0.5	0.5
Fourier Series for H										
a_1	c_6	b_6	c_7	b_7	c_8	b_8	c_9	b_9	c_{10}	b_{10}
–0.04	–0.39	–0.04	–0.01	0.086	–0.93	0.035	0.0187	–0.07	–0.1	–0.1
E =0.2545										

As compared, this group of results are not acceptable. The requirements are best met when 60 mm length is used.

2.2.3.4 Optimized Length 3D NTL Design

Here, the length d is set as an optimization variable. The results are as follow:

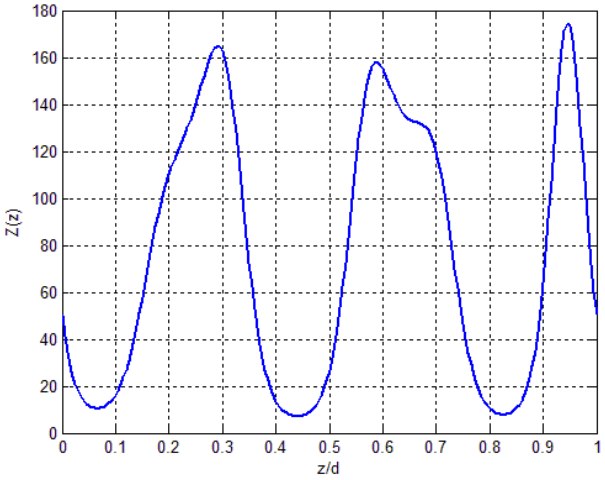

Figure 2.40. *Z*-Variation of Optimized Design

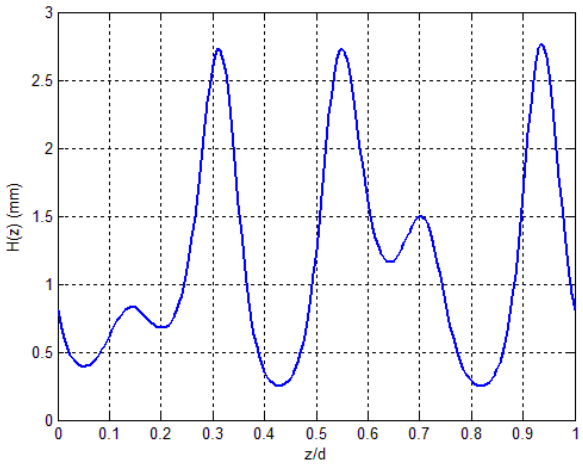

Figure 2.41. Thickness-Variation

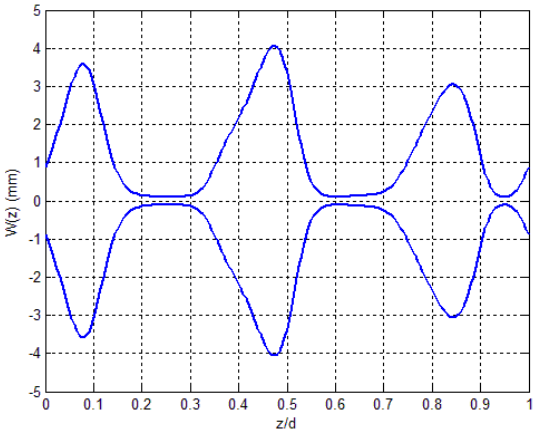

Figure 2.42. Width-Variation

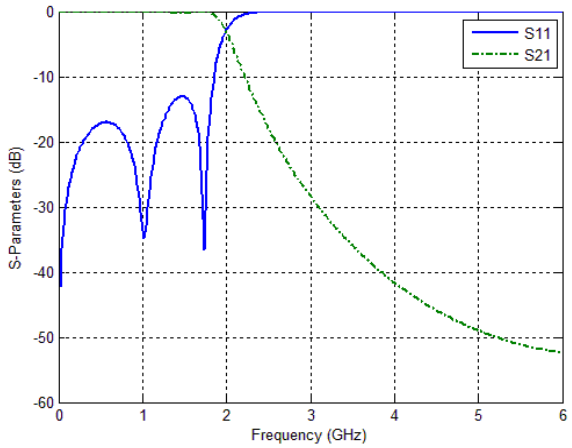

Figure 2.43. S-parameters

Figure 2.40. is the impedance value of optimized length design; Figure 2.41 is the thickness layout of 3D NTL design; Figure 2.42. is the width layout of 3D NTL design; Figure 2.43. is S-Parameter of 3D NTL design. For the analytical results, the width set and thickness set stay in the boundaries. Also the electrical responses are acceptable. Table 14 shows the coefficients of Fourier series for length-, width-, and thickness optimized structure.

Table 14 Coefficients of Fourier Series for 3D-Optimized Structure

Fourier Series for Z										
a_0	c_1	b_1	c_2	b_2	c_3	b_3	c_4	b_4	c_5	b_5
–0.04	–0.16	0.059	–0.39	0.443	0.625	–1.034	–1.034	–0.26	–0.14	–0.54
Fourier Series for H										
a_1	c_6	b_6	c_7	b_7	c_8	b_8	c_9	b_9	c_{10}	b_{10}
–0.04	0.1282	–0.17	–0.02	0.015	0.133	0.3644	–0.639	0.07	0.002	–0.4
E =0.0511										

The structure of length-, thickness- and width-optimized LPF is constructed and simulated as Figure 2.44.:

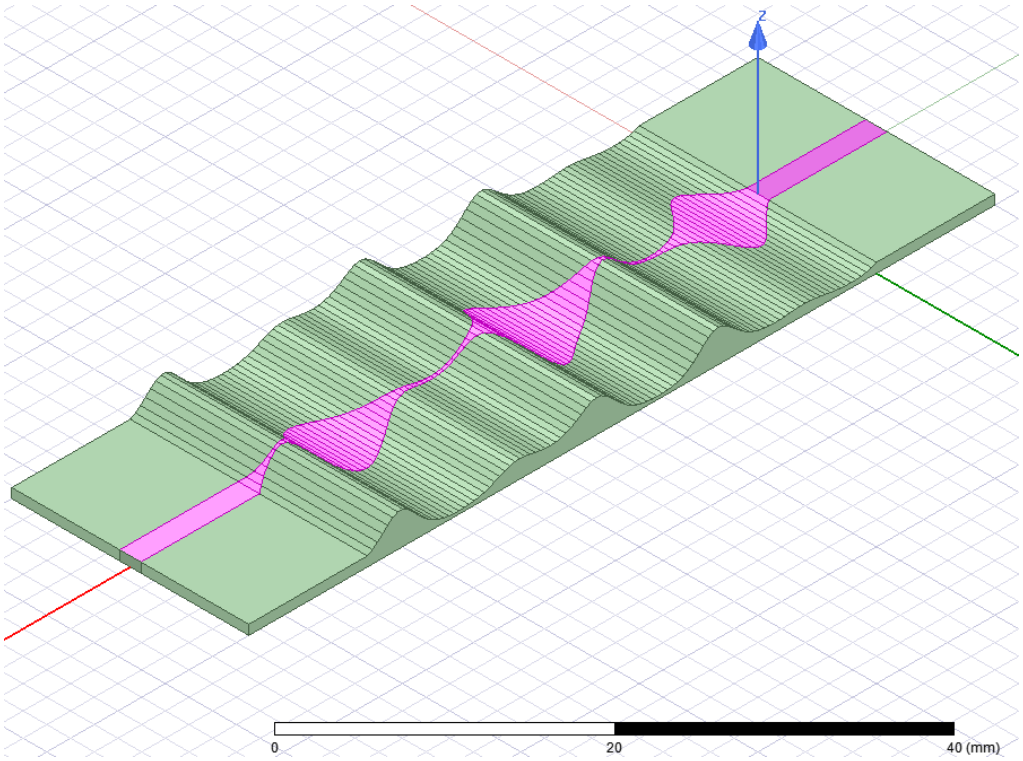

Figure 2.44. Structure of HFSS Simulation

Where the total length of the 3D-modified structure is 42.956 mm. Figure 2.45. shows the S-parameters of the simulation. S_{11} is greater than –13 dB in passband. When f_c = 6 GHz, S_{21} is –52 dB, which means the signal is fully filtered out.

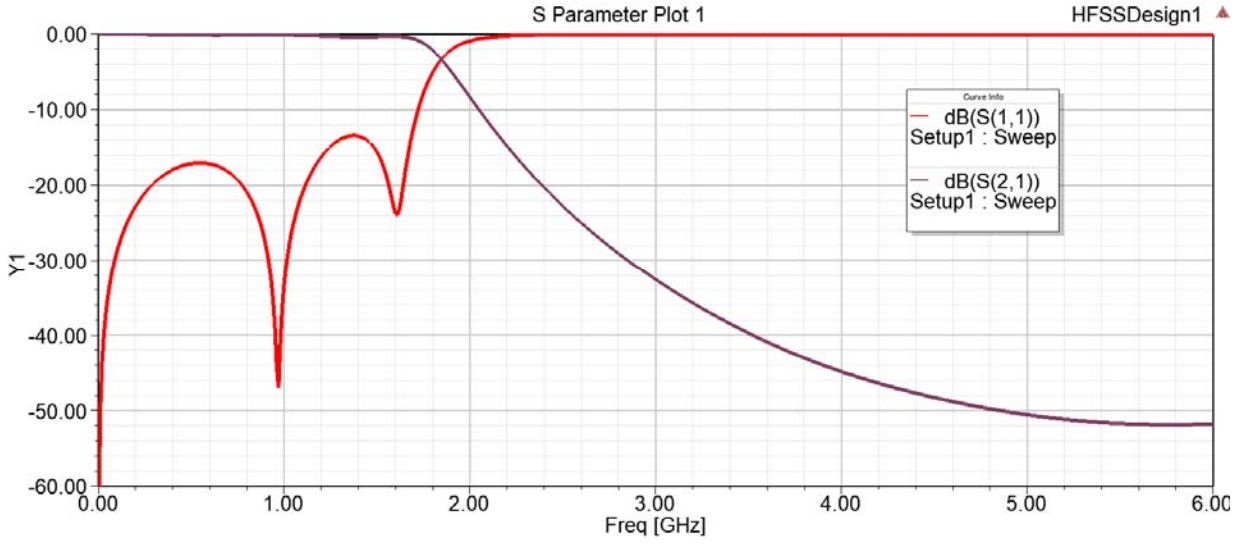

Figure 2.45. Electrical Responses of Optimized length 3D NTL

Figure 2.46. shows the comparison result of the conventional LPF design and the length-, thickness-, and width-optimized design.

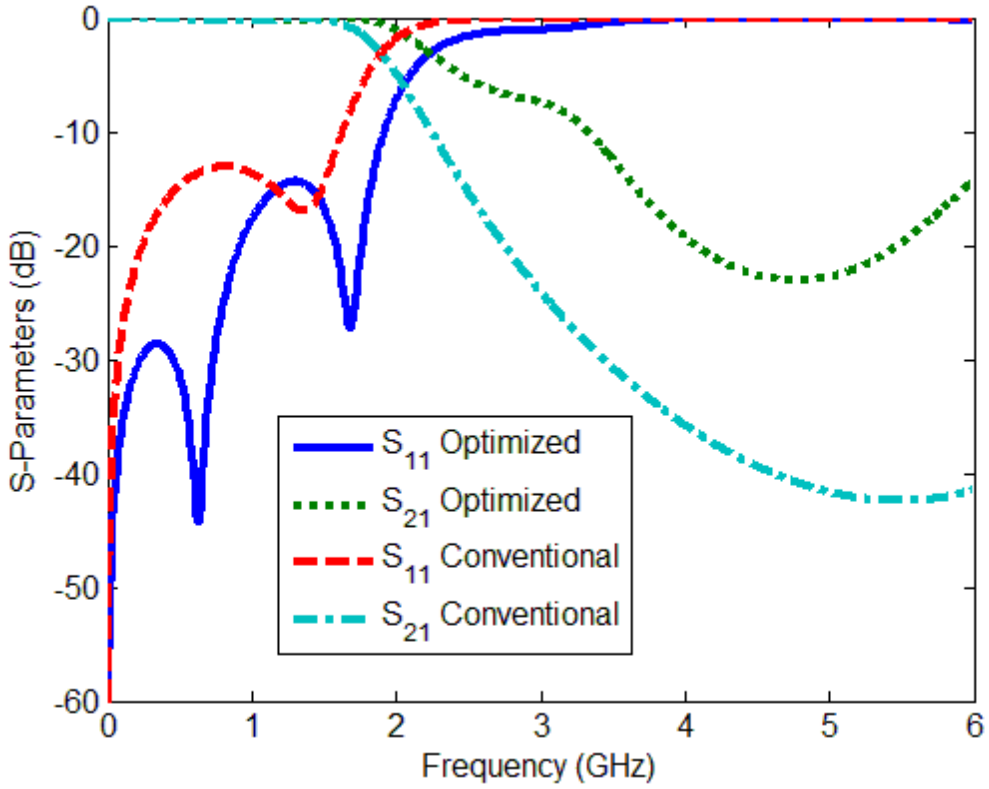

Figure 2.46. Simulation Result of Conventional LPF Design and 3D-Optimized Design.

Table 15 shows the comparison result of the conventional LPF design and the 3D optimized design. Hence, by keeping the same electrical responses in passband, the 3D optimized design is 29.83% shorter than the conventional LPF design.

Table 15 Comparison of Conventional and 3D-Modified-NTL (Length Included) based LPF

	S_{11}(dB)	Length(mm)
Conventional UTL-LPF	–13	71.58
Thickness, Width- and Length-Modified NTL-LPF	–13	42.95
Comparison	0	29.83%

CHAPTER 3. SUPERFORMULA BASED BANDPASS FILTER DESIGN

Driven by the research aiming to realize BPF with minimized size and enhanced electrical responses, SRR are used. In order to enhance the bandwidth, multi-order (single, dual, and triple) SRR based BPF are proposed.

In this section, a design procedure of a single-cell superformula shaped SRR based BPF is presented. The objective of this design is to achive the same (or better) electrical response as conventional SRR based filters with a reduced size in required operation band. Mathematical derivations, structure design, and results will be presented in sequence. Figure 3.1. shows the equivalent circuit of n-coupled resonators. *L* and *C* denote the inductance and capacitance, *n* is the maximum number of cells.

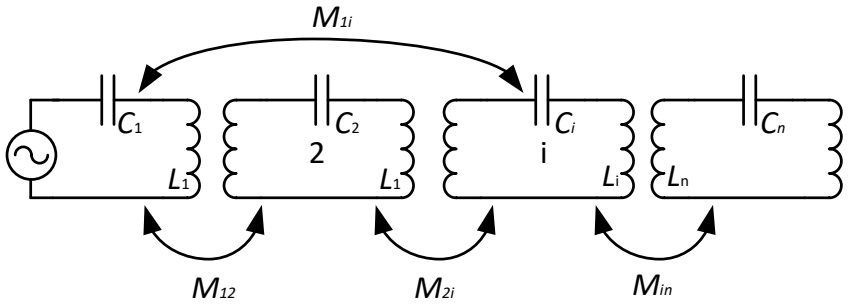

Figure 3.1. Equivalent Circuit of *n*-Coupled Resonators

3.1 Methodology

Firstly, for filters with only one pair of transmission zeros, from (3.1) to (3.12) equations are described in [53]. In which the transfer function of S_{21} shows as follows:

$$\left|S_{21}(\Omega)\right|^2 = \frac{1}{1+\varepsilon^2 F_x^2(\Omega)} \tag{3.1}$$

where Ω is the frequency variable normalized to the passband cut-off frequency, *x* is the degree of the filter, F_x is the filtering function, and ε is the ripple constant related to a given return loss L_R in dB, which is given as:

$$L_R = 20\log\left|S_{11}\right| \tag{3.2}$$

The definition of Ω could be given as:

$$\Omega = \frac{1}{FBW}\left(\frac{\omega}{\omega_0} - \frac{\omega_0}{\omega}\right) \tag{3.3}$$

where ω is the radian frequency variable of BPF, ω_0 is the midband radian frequency, and FBW is defined as the fractional bandwidth. It is worth to mention that $\Omega = \pm\Omega_a (\Omega_a > 1)$ are the frequencies of a pair of attenuation poles.

The transmission zeros of this type of filter may be realized by cross coupling a pair of nonadjacent resonators, the filter synthesis starts with the design parameters (g_i , γ , S, J_m):

$$g_i = \begin{cases} \dfrac{2\sin(\dfrac{\pi}{2n})}{\gamma}, & i = 1 \\ \dfrac{4\sin\dfrac{(2i-1)\pi}{2n}\sin\dfrac{(2i-3)\pi}{2n}}{\gamma^2 + \sin^2\dfrac{(i-1)\pi}{n}}, & i = 2,3,...,m, m = n/2 \end{cases} \tag{3.4}$$

and γ is given as:

$$\gamma = \sinh\left(\frac{1}{n}\sinh^{-1}\frac{1}{\varepsilon}\right) \tag{3.5}$$

The definition of *S* is given as:

$$S = \left(\sqrt{1+\varepsilon^2} + \varepsilon\right)^2 \tag{3.6}$$

and J_m is defined as:

$$J_m = 1/\sqrt{S} \tag{3.7}$$

In order to get transmission zero at $\Omega = \pm\Omega_a$, the required value of J_{m-1} is given by:

$$J_{m-1} = \frac{-J_m^{'}}{(\Omega_a g_m)^2 - J_m^{'2}} \tag{3.8}$$

where $J_m^{'}$ is interpreted parameter of J_m, which is expressed as:

$$J_m^{'} = \frac{J_m}{1 + J_m J_{m-1}} \tag{3.9}$$

Until equation (3.9), all of the design parameters are defined. Later on, coupling coefficients can be explained. Figure 3.2. shows the basic coupling structure of BPF:

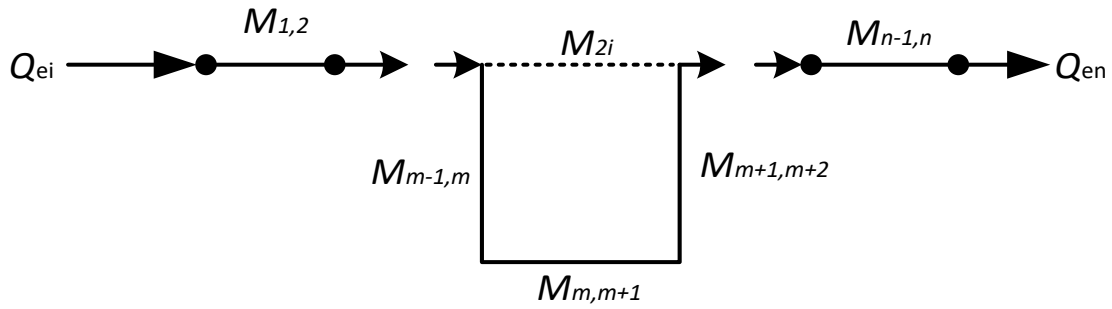

Figure 3.2. General Coupling Structure of BPF with Coupling Coefficients

The external quality factors of the input and output resonators (Q_{ei} and Q_{en}) are expressed as:

$$Q_{ei} = Q_{en} = \frac{g_1}{FBW} \tag{3.10}$$

with the design elements values (g_i , γ , S, J_m), coupling coefficient M is given as follows:

$$\begin{cases} M_{i,i+1} = M_{n-i,n-i+1} = \dfrac{FBW}{\sqrt{g_i g_{i+1}}} \\ M_{m,m+1} = \dfrac{FBW \cdot J_m}{g_m} \\ M_{m-1,m+2} = \dfrac{FBW \cdot J_{m-1}}{g_{m-1}} \end{cases} \tag{3.11}$$

In order to get a reduced-size layout, conventional square-SRR equation is replaced by superformula $r(\varphi)$ equation, which could be given as follows [48]:

$$r(\varphi) = \left(\left| \frac{\cos\left(\frac{q_1 \varphi}{4}\right)}{a} \right|^{p_2} + \left| \frac{\sin\left(\frac{q_2 \varphi}{4}\right)}{b} \right|^{p_3} \right)^{-\frac{1}{p_1}} \tag{3.12}$$

3.2 Structural Design

In this section, the physical and electrical parameters are analyzed. The purpose of the parametric analysis is to find the minimum SRR size. Corresponding to the physical limitations, the gaps between the different rings are no less than 0.1 mm. For multi-order SRRs, the seperation between the cells is at least 0.2 mm. The SRR based BPF is implemented on Rogers

RO4003C substrate with 0.813mm thickness, whose relative permittivity ε_r = 3.55, with a dielectric loss ($\tan\delta$) of 0.0027. Besides of physical constraints, other specifications also need to be considered. The cutoff frequency of BPF is set to 1.1 GHz. In superformula equation, $a = b = 1$, and $p_1 = p_2 = 1$, $p_2 = 8$ .Then, q values go through a parametric analysis, which lead to $q_1 = q_2 = 6$. These values are chosen after a parametric analysis procedure, where a and b values control the curvature between the bulges, q values control the number of the bulges, p values control curvature of each bulge.

3.3 SRR based BPF Results

A first order SRR based BPF is designed and simulated according to the design constraints, the physical parameters are obtained and imported into HFSS in Figure 3.3. Simulation result are shown in Figure 3.4.:

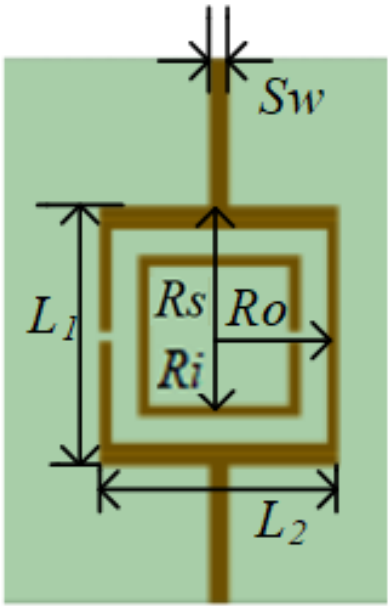

Figure 3.3. Single Cell SRR Based BPF Structure

Table 16 Physical Parameters of 1.1GHz SRR-BPF

Parameter		Value (mm)
Structure length	L_1	47.4
Structure width	L_2	45
Strip width	*Sw*	2
Outer ring radius	*Ro*	19
Inner ring radius	*Ri*	13
Strip ring radius	*Rs*	21.2

Table 16 shows the physical parameters of the conventional SRR based BPF. In Figure 3.4., the cutoff frequency is 1.1 GHz, S_{11} is better than –25 dB, and S_{21} is smaller than –1 dB in passband. S_{21} is –19 dB when f = 0.9 GHz, and its –20 dB when f = 1.3 GHz, the signal is filtered out in stopband. The bandwidth of BPF is 68.7 MHz with roll-off factor β_r = 0.67.

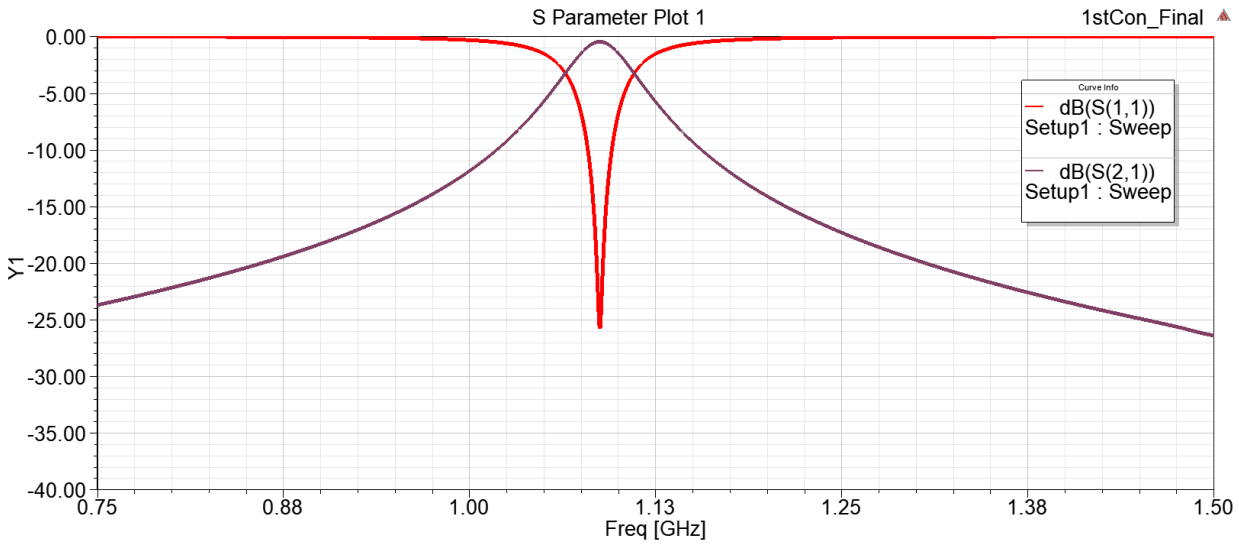

Figure 3.4. Single Cell SRR Based BPF Electrical Response

Also, SRR-BPF implemented with superformula shape is also simulated and generated as shown Figure 3.5.:

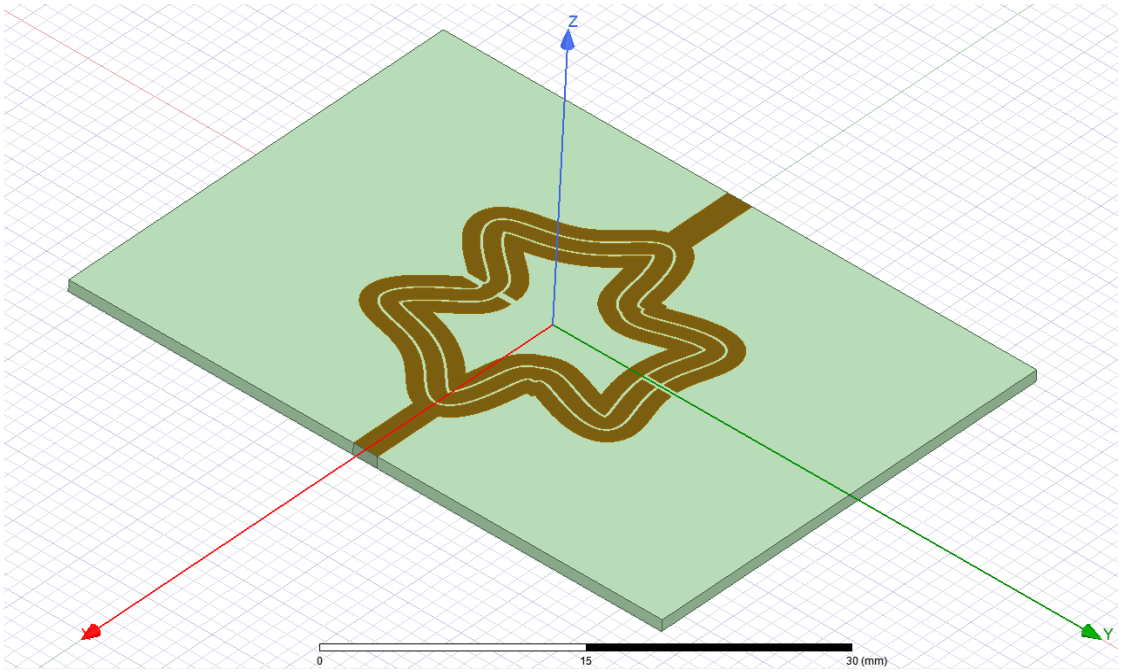

Figure 3.5. Single Cell Superformula Implemented SRR Structure

The electrical response of single cell superformula Implemented SRR-BPF is showing in Figure 3.6. The cutoff frequency is 1.1 GHz, S_{11} is better than –25 dB, and S_{21} is 0 dB at cutoff

frequency. S_{21} is –17 dB when f = 0.9 GHz, and its –17 dB when f = 1.3 GHz, the signal is filtered out in stopband. The bandwidth of this BPF design is 51.2 MHz with β_r = 0.69.

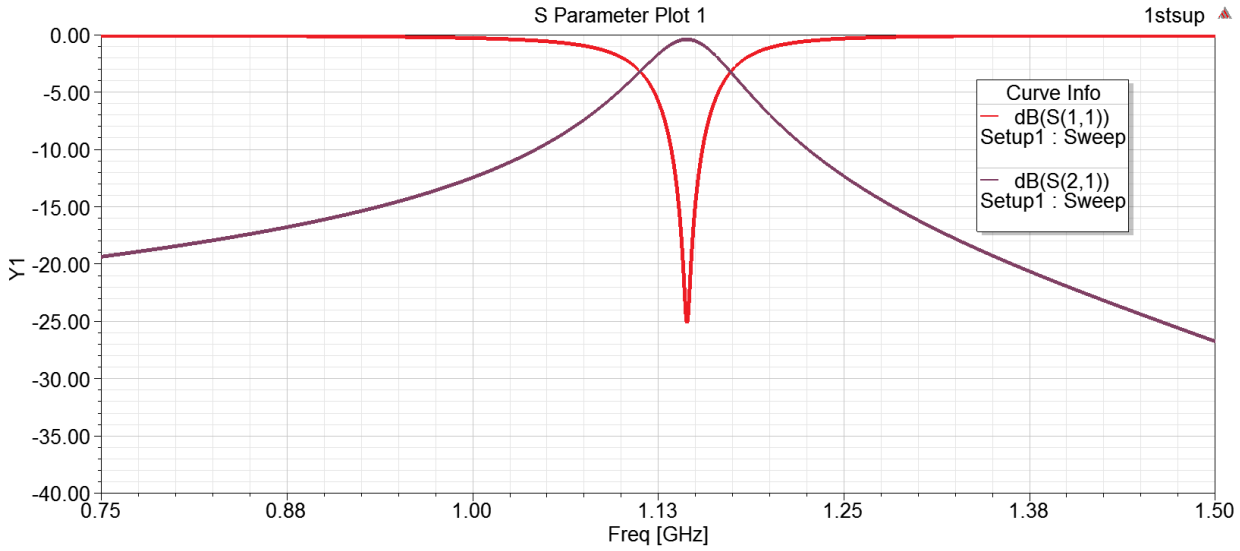

Figure 3.6. Single Cell Superformula Implemented SRR-BPF Simulation Result

Table 17 shows the comparison result of the conventional SRR-BPF design and superformula based SRR-BPF, where 'S_{11}' is S_{11} value at cutoff frequency. Hence, by keeping same electrical response in passband, the superformula based SRR-BPF is 18.36% smaller than the conventional SRR-BPF design.

Table 17 Comparison of Conventional/Superformula based SRR-BPF Design

	S_{11}(dB)	Area(mm^2)
Conventional SRR-BPF	–25	444
Superformula based SRR-BPF	–25	362.48
Comparison	0	18.36%

In order to enhance the bandwidth, as well as improve roll-off factor, multi-order SRR-BPF are designed. Figure 3.7. shows the physical parameters of the second-order conventional SRR based BPF. Table 18 shows physical parameters of second-order SRR-BPF.

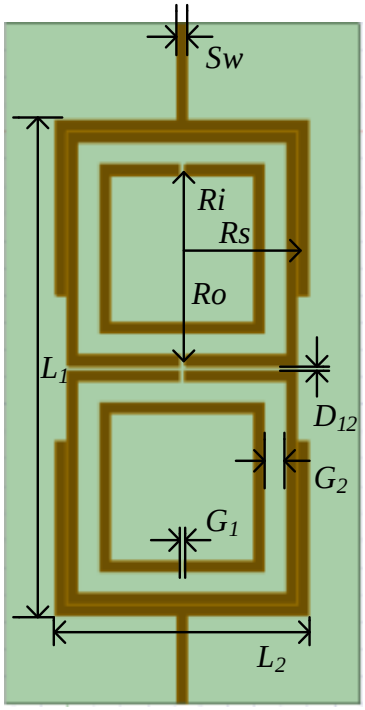

Table 18 Physical Parameters of 1.1GHz 2nd-Order SRR-BPF

Parameter		Value(mm)
Structure length	L_1	91.1
Structure width	L_2	47.4
Strip width	*Sw*	2
Strip ring radius	*Rs*	21.2
Outer ring radius	*Ro*	19
Inner ring radius	*Ri*	13
Gap inside ring	G_1	0.7
Gap between ring	G_2	4
Distance 1&2	D_{12}	0.7

Figure 3.7. Second-Order SRR based BPF Structure

Moreover, the electrical response of second-order conventional SRR-BPF is showing in Figure 3.8. The cutoff frequency is 1.1 GHz, S_{11} is better than –15 dB, and S_{21} is smaller than –1 dB at cutoff frequency. S_{21} is –40 dB when f = 0.9 GHz, and its –37 dB when f = 1.3 GHz, the signal is filtered out in stopband. The bandwidth of this BPF design is 84.2 MHz with β_r = 0.61.

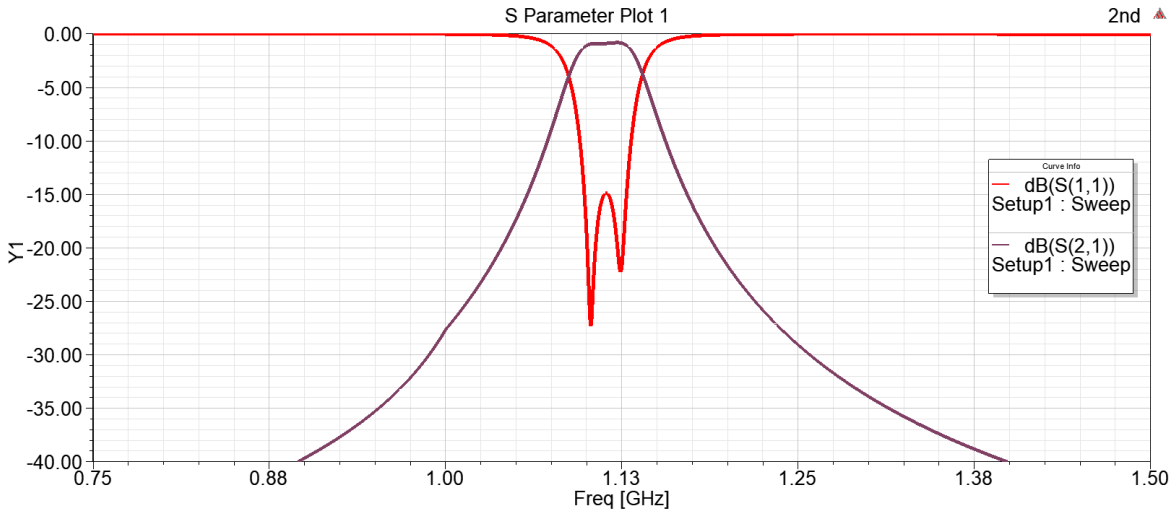

Figure 3.8. Second-Order SRR based BPF Result

The structure of second-order superformula Implemented SRR-BPF is showing in Figure 3.9.

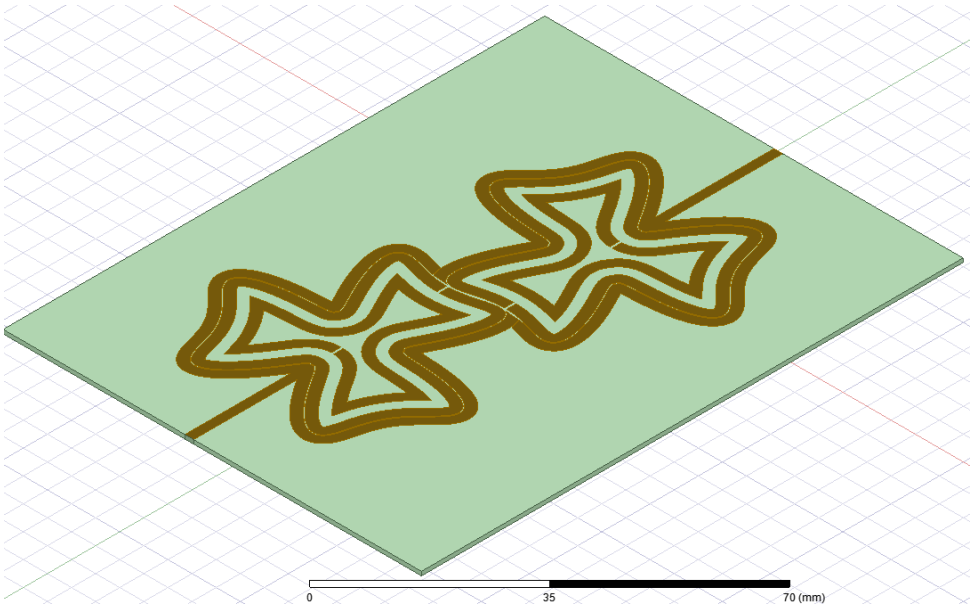

Figure 3.9. Superformula Implemented Second-Order SRR based BPF Structure

The electrical response of second-order superformula Implemented SRR-BPF is showing in Figure 3.10. The cutoff frequency is 1.1 GHz, S_{11} is better than –19 dB, and S_{21} is –1 dB at cutoff frequency. S_{21} is –24 dB when f = 0.9 GHz, and its –27 dB when f = 1.3 GHz, the signal is filtered out in stopband. The bandwidth of this BPF design is 56.5 MHz with β_r = 0.57.

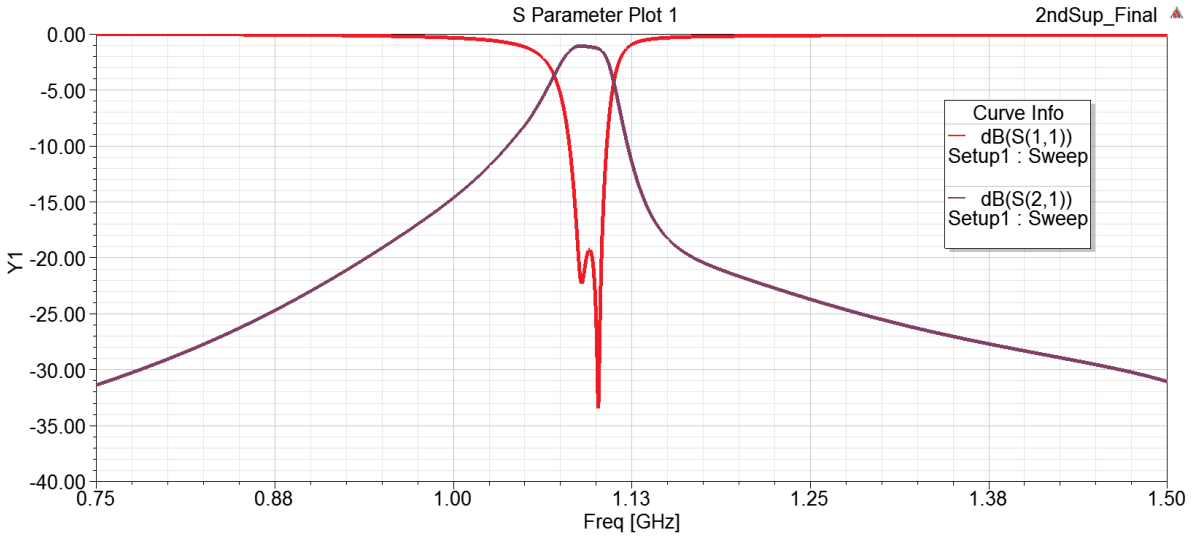

Figure 3.10. Second-Order Superformula Implemented SRR based BPF result

Table 19 shows comparison of 2nd order conventional/superformula based SRR-BPF design.

Table 19 Comparison of 2nd order Conventional/Superformula based SRR-BPF Design

	S_{11}(dB)	Area(mm^2)
Conventional SRR-BPF	-15	4318.14
Superformula based SRR-BPF	-19	3899.24
Comparison	4	9.7%

Based Figure 19, the passband value of S_{11} in sperformula implemented single SRR-BPF is 4 dB greater conventional design. Based on Table 19, the superformula implemented SRR structure area is 19.7% smaller than conventional one. The structure of third-order conventional SRR-BPF is showing in Figure 3.11.

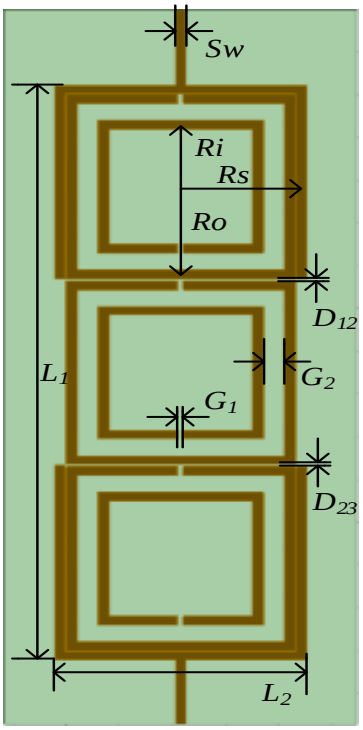

Figure 3.11. Third-Order Conventional SRR Based BPF Structure

Table 20 Physical Parameters of 1.1GHz 3rd-Order SRR-BPF

Parameter		Value(mm)
Structure length	L_1	134.5
Structure width	L_2	47.4
Strip width	*Sw*	2
Strip ring radius	*Rs*	21.2
Outer ring radius	*Ro*	19
Inner ring radius	*Ri*	13
Gap inside ring	G_1	0.5
Gap between ring	G_2	4
Distance 1&2	D_{12}	0.58
Distance 2&3	D_{23}	0.52

Figure 3.12. shows S_{11} is better than –12 dB, and S_{21} is smaller than –1 dB at f = 1.1 GHz. S_{21} is –67 dB when f = 0.9 GHz, and its –65 dB when f = 1.3 GHz, the signal is filtered out in stopband. The bandwidth of this BPF design is 92.8 MHz with β_r = 0.48.

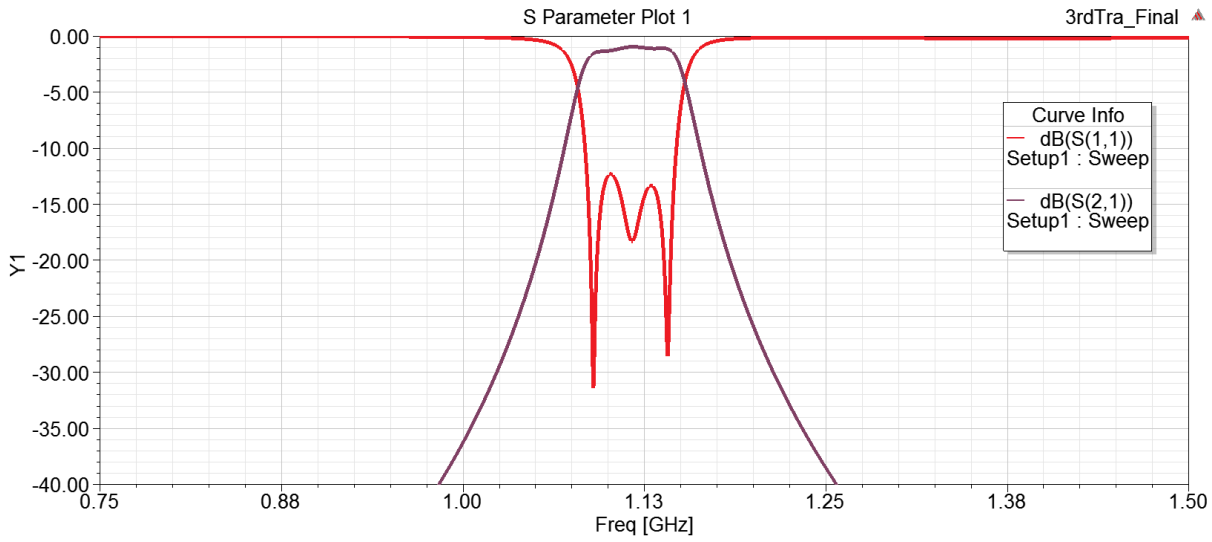

Figure 3.12. Third-Order Conventional SRR based BPF Result

The physical structure of third-order superformula based SRR-BPF is showing in Figure 3.13.

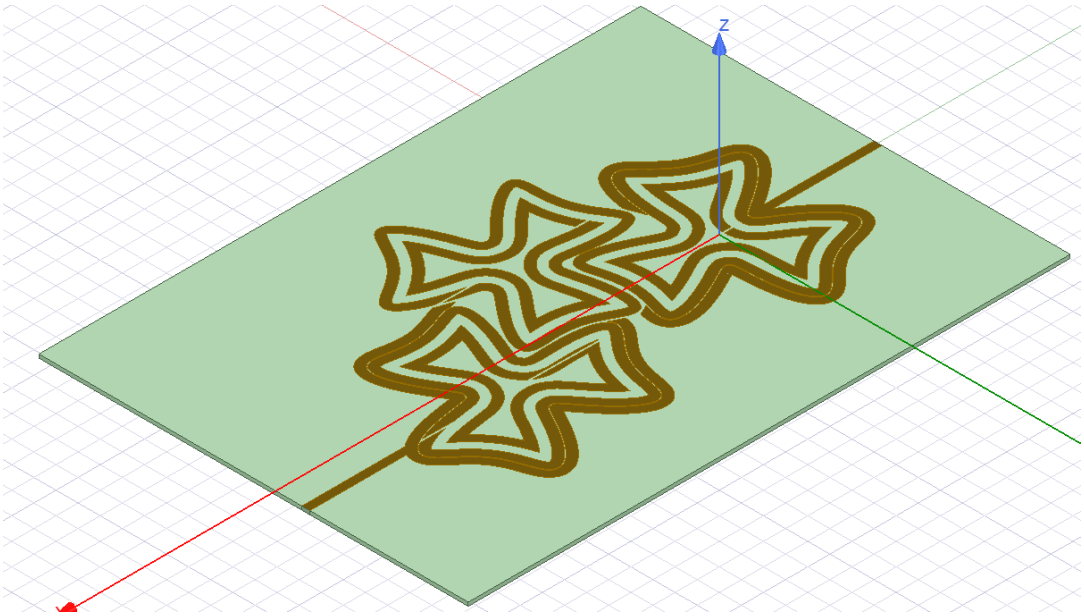

Figure 3.13. Third-Order superformula Based SRR-BPF Structure

The electrical response of second-order superformula implemented SRR-BPF is showing in Figure 3.14. It shows the cutoff frequency is 1.1 GHz, S_{11} is better than –13 dB, and S_{21} is smaller than –1 dB at cutoff frequency. S_{21} is –58 dB when f = 0.9 GHz, and its –61 dB when f = 1.3 GHz, the signal is filtered out in stopband. The bandwidth of this BPF design is 68.1 MHz with β_r = 0.52.

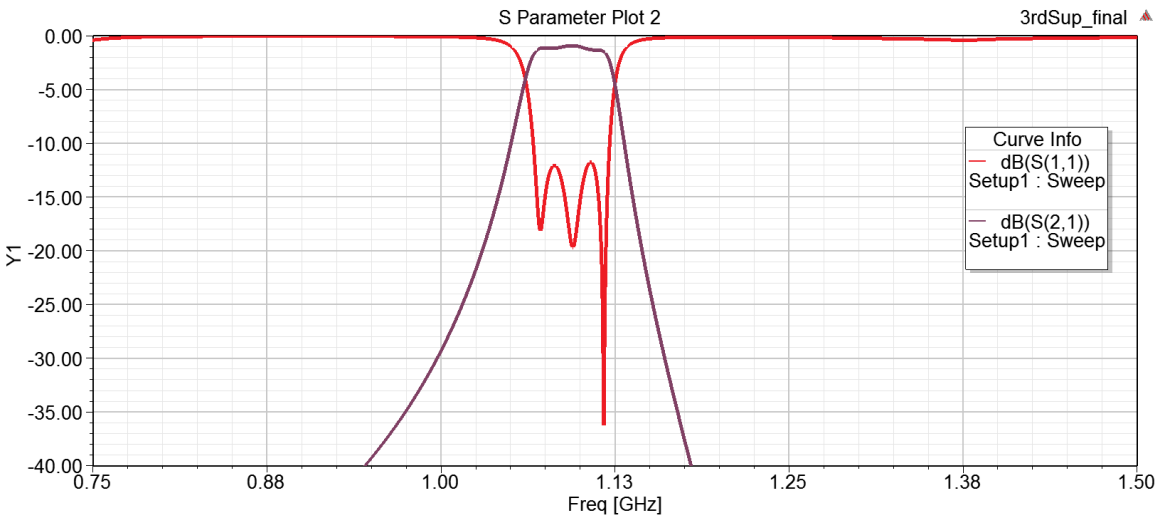

Figure 3.14. Third-Order superformula Based SRR-BPF Result

Based on Figure 3.11. and Figure 3.13., the of S_{11} value in passband of sperformula implemented single SRR-BPF is as same as conventional ones. Table 21 shows comparison of conventional/superformula based SRR-BPF design. Based on Table 21, the superformula implemented SRR structure area is 5.69% smaller than conventional one.

Table 21 Comparison of 3rd order Conventional/Superformula based SRR-BPF Design

	S_{11}(dB)	Area(mm^2)
Conventional SRR-BPF	-13	6375.3
Superformula based SRR-BPF	-13	6031.8
Comparison	0	5.69%

Table 22 declaims bandwidth, roll-off factor, and size reduction for all designs.

Table 22 Physical Parameters of 1.1GHz SRR-BPF

	Bandwidth(MHz)		Roll-off factor (β_r)		Size Reduction(%)
	Conventional Design	Superformula based Design	Conventional Design	Superformula based Design	
1st order	68.7	51.2	0.67	0.69	18.36
2nd order	84.2	56.5	0.61	0.57	9.7
3rd order	92.8	68.1	0.48	0.52	5.69

CHAPTER 4. CONCLUSIONS

The proposed systematic methodology and parametric analysis are to achieve a non-uniform transmission line based LPF, as well as superformula based BPF. The conventional uniform microstrip transmission line is replaced by a length- and width-varying transmission line, and a thickness-varying substrate using truncated Fourier series. The width-varying NTL-LPF design keeps the same electrical response as conventional stepped impedance LPF with a 12.8% length reduction. The 3-dimension modified (width and thickness) NTL-LPF design gains the same electrical response with a 19.3% length reduction. For length-, width, and thickness-modified NTL, the electrical response is as same as conventional design with a 29.83% length deduction.

Moreover, the conventional square-SRR based BPF is replaced by a superformula shape. By using parametric analysis, a BPF with 1.1 GHz cutoff frequency is analyzed and simulated. For the first order, S_{11} value in passband of superformula based SSR-BPF is greater than –25 dB. The parametric analysis design obtains the same result as conventional SRR based BPF with 18.36% size reduction. Furthermore, S_{11} value in passband of dual-order design is 4 dB better than conventional design, and the size of SRR-BPF obtains 9.7% size reduction. As for triple-order SRR design, S_{11} value in passband of dual-order keeps same electrical response as conventional design, whose size-reduction is 5.69%.

Hence, mathematical and theoretical analysis is established, optimized, and the resulting miniaturized filters are simulated. Analytical and simulated results are in a good agreement and outperform conventional designs in terms of size and filtering response.

As an extension for this thesis, multiple ideas can be considered. For example, superformula shape could be implemented not only on SRR designs, but also on other components (i.e., antennas, coplanar waveguides, complementary SRRs) as applying superformula shapes remarkably reduced the area of SRR based BPFs in this thesis. Furthermore, third-order SRR is the highest order in this thesis, hence going through parametric analysis of higher order (i.e., Quad, Quint) BPFs is possible.

REFERENCES

[1] Charles E. Smith, Ray-Sun Chang: 'Microstrip Transmission Line With Finite-Width Dielectric and Ground Plane' March 9, 1985, 9.

[2] Savita Maurya: 'An Extensive Study, Design And Simulation Of Mems Guided Media: Microstrip Line' International Journal on Smart Sensing And Intelligent Systems, 2010, 3, (1).

[3] R. Kalyan, K. T. Reddy, K. Padma Priya: 'Novel UWB microstrip antenna with dual band-notched characteristics for short distance wireless applications' Journal of Engineering Technology, 2018, 1, (1), pp. 584-594.

[4] Gerardo Aranguren, Josu Etxaniz, Luis A. López-Nozal: 'Design of Printed Circuit Boards in University' Technologies Applied to Electronics Teaching, 2012, 10.1109/TAEE.2012.6235397.

[5] Kenneth H. Church, Harvey Tsang, Ricardo Rodriguez, Paul Defembaugh: 'Printed Circuit Structures, The Evolution Of Printed Circuit Boards' IPC APEX EXPO Conference, 2013.

[6] Pingjuan Zhang, Minquan Li: 'A Novel Sharo Roll-Off Microstrip Lowpass Filter With Improved Stopband And Compact Size Using Dual-Plane Structure' Microwave And Optical Technology Letters, 2016, 58, (5).

[7] Anand K. Verma, Nainu P. Chaudhari, Ashwani Kumar: 'High Performance Microstrip Transverse Resonance Lowpass Filter' Microwave And Optical Technology Letters, 2012, 55, (5)

[8] Vamsi Krishna Velidi, Subrata Sanyal: 'High-Rejection Wide-Stopband Lowpass Filters Using Signal Interference Technique' Inc. Int J RF and Microwave CAE, 2010, 20, pp. 253–258.

[9] Prachi Tyagi: 'Design and Implementation of Low Pass Filter using Microstrip Line' International Journal of Latest Trends in Engineering and Technology (IJLTET), 2015, 3, (5).

[10] Hussein Shaman, Sultan Almorqi, Ahmed Alamoudi: 'Composite Microstrip Lowpass Filter With Ultrawide Stopband And Low Insertion Loss' Microwave And Optical Technology Letters, 2010, 57, (4).

[11] P. M. Raphika, P. Abdulla, P. M. Jasmine:' Compact Lowpass Filter With A Sharp Roll-Off Using Patch Resonators' Microwave And Optical Technology Letters, 2014, 56, (11).

[12] J.-M. Zhou, L.-H. Zhou, H. Tang, Y.-J. Yang, J.-X. Chen, Z.-H. Bao: 'Novel Compact Microstrip Lowpass Filters With Wide Stopband Using Defected Ground Structure' J. Of Electromagn. Waves And Appl., 2011, 25, Pp. 1009–1019.

[13] Bhagirath Sahu, Soni Singh, Manoj Kumar Meshram, S. P. Singh: 'Study of compact microstrip lowpass filter with improved performance using defected ground structure' Int J RF Microw Comput Aided Eng, 2018, 28, (e29).

[14] Mohammed A. Aseeri: 'Compact Microstrip Lowpass Filter with Low Isertion Loss for UWB Medical Applications' Wireless Communications and Mobile Computing, 2018.

[15] Vivek Singh Kushwah, Geetam S. Tomar, Sarita Singh Bhadauria: 'Designing Stepped Impedance Microstrip Low-Pass Filters Using Artificial Neural Network at 1.8 GHz' Communication Systems and Network Technologies (CSNT), 2013.

[16] Lingyu Li, Haiwen Liu, Baohua Teng, Zhiguo Shi, Wenming Li, Xiaohua Li, and Shuxin Wang: 'Novel Microstrip Lowpass Filter Using Stepped Impedance Resonator And Spurline Resonator' Microwave And Optical Technology Letters, 2009, 51, (1).

[17] Sukumar Chandra, Tapas Misra: 'Design of a 4^{th} Order Low-Pass Butterworth Filter' Research Journal of Science Engineering and Technology, 2015, 5, (4).

[18] Liew Hui Fang, Syed Idris Syed Hassan, Mohd Fareq Abd. Malek: 'Design of UHF Harmonic Butterworth Low Pass Filter For Portable 2 ways-Radio' International Conference on Electronic Design, 2014.

[19] Prashant Kumar Singh, Anjini Kumar Tiwary, Nisha Gupta: 'Ultra-Compact Switchable Microstrip Band-Pass Filter– Low-Pass Filter With Improved Characteristics' Microwave And Optical Technology Letters, 2017, 59, (1).

[20] Mudrik Alaydrus: Analysis of low pass filter using nonhomogeneous transmission lines' International Conference on Information and Communication Technology (ICoICT), 2014.

[21] Said Attamimi, Mudrik Alaydrus: 'Design of Chebychev's Low Pass Filters Using Nonuniform Transmission Lines' J. ICT Res. Appl., 2015, 9, (3).

[22] Ibtissem Oueriemi, Fethi Choubani, Isabelle Huynen: 'Performance of Low-pass Filter based on non-uniform Capacitor Sections' 5th International Conference on Design & Technology of Integrated Systems in Nanoscale Era, 2010.

[23] Jimmy Hester, Evan Nguyen, Jesse Tice, Vesna Radisic: 'A Novel 3D-Printing-Enabled "Roller Coaster" Transmission Line' 2017 IEEE International Symposium on Antennas and Propagation, 2017.

[24] X,C Zhang, J.Xu: 'Design of Quasi-Elliptic Bandpass Filter Based on Slow Wave Open-Loop Resontors' J. of Electromagn. Waves and Appl., 2008, 22, (12), pp. 1849-1856.

[25] Jia-Sheng Hong: 'Theory and Experiment of Novel Microstrip Slow-Wave Open-Loop Resonator Filters' IEEE transactions on microwave theory and techniques, 1997, 45, (12).

[26] Md. Rokunuzzaman, Mohammad Tariqul Islam: 'Design of a Compact Dual-BandBand-Pass Filter for Global Positioning System and Fixed Satellite Applications' 8th International Conference on Electrical and Computer Engineering, 2014.

[27] Kongpop U-yen, Edward J. Wollack: 'A Planar Bandpass Filter Design With Wide Stopband Using Double Split-End Stepped-Impedance Resonators' IEEE Transactions On Microwave Theory And Techniques, 2006, 54, (3).

[28] Azzedin Naghar, Otman Aghzout, Ana Vazquez Alejos: 'Design Of Compact Wideband Multi-Band And Ultrawideband Band Pass Filters Based On Coupled Half Wave Resonators With Reduced Coupling Gap' IET Microwaves, Antennas & Propagation, 2015, 1751-8725.

[29] Sugchai Tantiviwat, Siti ZURAIDAH Ibrahim: 'Miniature Microstrip Bandpass Filters Based On Quadruple-Mode Resonators With Less Via' IEEE MTT-S International Conference on Microwaves for Intelligent Mobility, 2017, 978-1-5090-4354-5/17.

[30] Igwue. G. A,: 'Implementation of a Sixth Order Active Band-pass R-Filter', International Journal of Scientific & Engineering Research, 2014, 5, (4).

[31] M. Khodier: 'Design And Optimization Of Single, Dual, And Triple Band Transmission Line Matching Transformers For Frequency-Dependent Loads' ACES Journal, 2009, 24, (5).

[32] Philippe Gay-Balmaz: 'Electromagnetic Resonances in Individual and Coupled Split Ring Resonators' Journal of applied physics, 2002, 92, (5), 2929/8.

[33] Achmad Munir: 'Development of Dual-Band Microstrip Bandpass Filter Based on Split Ring Resonator' IEEE Publications, 2016, 978-1-4673-9811-4-16.

[34] Lavanya.G: 'Harmonic Suppression Bandpass Filter Using Square CSRR' IEEE 2nd Internetional Conference Publications, 2015.

[35] Hicham Megnafi, Noireddine boukli: 'An Efficient Analysis Of Microstrip Trisection Filters Using An Iterative Method Combined By Approach Multi-Scale' 2011, 11th Mediterranean Microwave Symposium (MMS).

[36] S. Vefesna, M. Saed: 'Compact Two-Layer Microstrip Bandpass Filter Using Broadside Coupled Resonators' Progress In Electromagnetics Research B, 2012, 37, pp. 87-102.

[37] X. Lai, Q. Li, P. Y. Qin: 'A Novel Wideband Bandpass Filter Based on Complementary Split Ring Reasonator' Progress In Electromagnetics Research C, 2008, 1, pp. 177-184.

[38] Vaishali Rathore, Seema Awasthi, Animesh Biswas: 'Design of Compact Dual-Band Bandpass Filter using Frequency Transformation and its Implementation with Split Ring resonator' 2016, 44th European Microwave Conference.

[39] Yongjun Huang, Guangjun Wen: 'Systematical Analysis For The Mixed Couplings For Two Adjacent Modified Split Rign Resonators And The Application To Cpmpact Microstrip Bandpass Filters' 2014, 107119, AIP Advances 4.

[40] S. Zahertar, A. D. Yalcinkaya: 'Rectangular Split-Ring Resonators With Single-Split And Two-Splits Under Different Excitations At Microwave Frequencies' 2015, 117220, AIP Advantages 5.

[41] Ahmed Rhbanou, Seddik Bri, Mohamed Sabbane: 'Design of Substrate Integerated Waveguide Bandpass Filter Based on Metamaterials CSRRs' Electrical and Electronic Engineering, 2014, 4, (4), pp. 63-72.

[42] Ahmed A. Ibrahim, Mahmoud A. Abdalla, Adel B. Abdel-Rahman: 'Wireless Bandpass Filters Build on Metamaterials' Microwave and Rf, 2018, 57, (5).

[43] Mushtaq A. Alqaisy, F. Sh. Khalifa: 'A Dual-Band Bandpass Filter using Single Unit Cell of Complementary Split Ring Resonator with Third Harmonic Reduction' Al-Sadeq International Conference on Multidisciplinary in IT and Communication Science and Applications, 2016, 9-10.

[44] Lakhan Singh, P. K. Singhal: 'Design and Comparision of Band Pass Cascade Trisection Microstrip Filter' The International Journal Of Engineering And Science, 2013, 2319–1813.

[45] Jordi Naqui, Miguel Durán-Sindreu: 'Novel Sensors Based on the Symmetry Properties of Split Ring Resonators' Sensors, 2011, 11, 7545-7553.

[46] Ferran Martín, Jordi Bonache: 'Application of RF-MEMS-Based Split Ring Resonators (SRRs) to the Implementation of Reconfigurable Stopband Filters: A Review' Sensors 2014, 14, 22848-22863.

[47] Badr Nasiri, Ahmed. Errkik, Jamal Zbitou, Abdelali Tajmouati, Larbi El Abdellaoui , Mohamed Latrach: 'A New Compact Microstrip Band-stop Filter by Using Square Split Ring Resonator' International Journal of Microwave and Optical Technology, 2017, 12, (5).

[48] Johan Gielis: 'A Generic Geometric Transformation That Unifies A Wide Range Of Natural And Abstract Shapes' American Journal of Botany, 2003, 90, (3), pp. 333-338.

[49] Ricardo Chacon: 'A Mathematical Description Of Natural Shapes In Our Nonlinear World' Apartado Postal 3812, 2018, E-06071.

[50] Zephaniah Hill, Jack McShane, Roman Zapata, Khair Al Shamaleh: 'Superformula-Inspired Split Ring Resonators with Applications to Compact Bandpass filters' 2019 International Applied Computational Electromagnetics Society Symposium.

[51] Enrique J. Rubio Marine-Duenas: 'Electromagnetic Modeling And Design Of A Novel Class Of Complementary Split Ring Resonators' International Journal of RF and MICROWAVE Computer-Aided Engineering, 2018, 10.1002/mmce.21582.

[52] David M. Pozar: 'Microwve Engineering' Wiley, 4th edn., 2011.

[53] Jia-Sheng Hong: 'Microstrip Filters for RF/Microwave Applications' Wiley, 2nd edn., 2010